AD-A090 097 ADVISORY GROUP FOR AEROSPACE RESEARCH AND DEVELOPMENT--ETC F/G 20/4
REPORT ON A COOPERATIVE PROGRAMME ON ACTIVE FLUTTER SUPPRESSION--ETC(U)
AUG 80 C HWANG, E H JOHNSON, G R MILLS
UNCLASSIFIED AGARD-R-689 NL

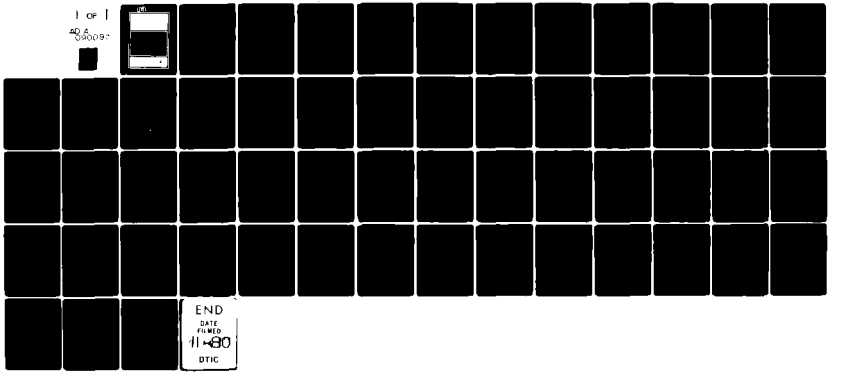

END
DATE FILMED
11-80
DTIC

AGARD-R-689

AGARD

ADVISORY GROUP FOR AEROSPACE RESEARCH & DEVELOPMENT

7 RUE ANCELLE 92200 NEUILLY SUR SEINE FRANCE

AGARD REPORT No. 689

Report on a Cooperative Programme on Active Flutter Suppression

NORTH ATLANTIC TREATY ORGANIZATION

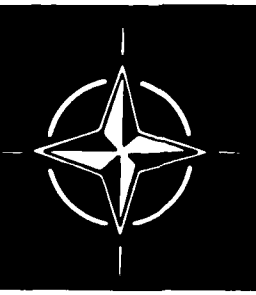

DISTRIBUTION AND AVAILABILITY ON BACK COVER

NORTH ATLANTIC TREATY ORGANIZATION

ADVISORY GROUP FOR AEROSPACE RESEARCH AND DEVELOPMENT

(ORGANISATION DU TRAITE DE L'ATLANTIQUE NORD)

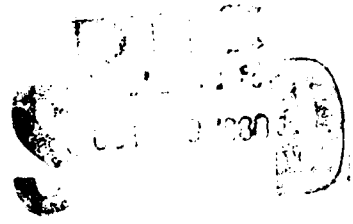

AGARD Report No.689

REPORT ON A COOPERATIVE PROGRAMME ON ACTIVE FLUTTER SUPPRESSION

Papers presented at the 50th Structures and Materials Panel Meeting, held in Athens, Greece, April 1980.

THE MISSION OF AGARD

The mission of AGARD is to bring together the leading personalities of the NATO nations in the fields of science and technology relating to aerospace for the following purposes:

- Exchanging of scientific and technical information;
- Continuously stimulating advances in the aerospace sciences relevant to strengthening the common defence posture;
- Improving the co-operation among member nations in aerospace research and development;
- Providing scientific and technical advice and assistance to the North Atlantic Military Committee in the field of aerospace research and development;
- Rendering scientific and technical assistance, as requested, to other NATO bodies and to member nations in connection with research and development problems in the aerospace field;
- Providing assistance to member nations for the purpose of increasing their scientific and technical potential;
- Recommending effective ways for the member nations to use their research and development capabilities for the common benefit of the NATO community.

The highest authority within AGARD is the National Delegates Board consisting of officially appointed senior representatives from each member nation. The mission of AGARD is carried out through the Panels which are composed of experts appointed by the National Delegates, the Consultant and Exchange Programme and the Aerospace Applications Studies Programme. The results of AGARD work are reported to the member nations and the NATO Authorities through the AGARD series of publications of which this is one.

Participation in AGARD activities is by invitation only and is normally limited to citizens of the NATO nations.

Published August 1980

ISBN 92-835-0270-2

Printed by Technical Editing and Reproduction Ltd
Harford House, 7–9 Charlotte St, London, W1P 1HD

PREFACE

Four short presentations were made to the Sub-Committee on Aeroelasticity, during the 50th Meeting of the Structures and Materials Panel, on the results of a cooperative programme on active flutter suppression on a dynamic model of the YF-17 aircraft.

During this programme, British Aerospace, MBB, Northrop, Air Force Flight Dynamics Laboratory, NASA and ONERA cooperated in deriving control laws for active flutter suppression for one explosive wing-store flutter case of the model. Phase control laws were all tested and compared during wind tunnel tests performed in the Langley 16 ft wind tunnel in October 1979. Results were quite promising and open the way for future cooperation on full-scale aircraft.

The Sub-Committee on Aeroelasticity unanimously agreed that the four presentations should be published as an AGARD Report since they were thought to be an important contribution to the development of active control technology.

G.COUPRY
Chairman, Sub-Committee
on Aeroelasticity

CONTENTS

WIND TUNNEL TEST OF A FIGHTER AIRCRAFT WING/STORE FLUTTER SUPPRESSION SYSTEM - AN INTERNATIONAL EFFORT

C. Hwang, E. H. Johnson, G. R. Mills
Northrop Corporation
Aircraft Group
Hawthorne, California 90250

T. E. Noll
Air Force Flight Dynamics Laboratory
Wright-Patterson Air Force Base, Ohio 45433

M. G. Farmer
NASA Langley Research Center
Hampton, Virginia 23665

SUMMARY

A 30% scale, half span model of a lightweight fighter aircraft with an active wing/store flutter suppression system was tested in the NASA Langley Research Center Sixteen Foot Transonic Dynamics Tunnel in September-October 1979. The test featured a store configuration that was intentionally designed to exhibit a violent flutter condition. In addition to Northrop organized control laws, three European countries also contributed control laws to stabilize this condition. After the control laws were mechanized by Northrop, they were tested at the Langley facility. The model was tested up to 170% of the open loop flutter dynamic pressure in a number of cases, with the indication that a substantially greater improvement was achievable. This paper discusses some special features of the test model, the design and implementation of the control laws, the test monitoring techniques and detailed test results.

INTRODUCTION

Wing/store flutter problems continue to degrade the performance of fighter-attack aircraft with air-to-ground combat roles. Flutter speed placards caused by the carriage of many combinations of external store configurations have reduced aircraft speed capability and as a result, decreased its survivability. Active flutter suppression has shown promise of preventing store flutter and has the potential for providing significant improvements in aircraft operational and mission effectiveness. Since flutter suppression systems can use electro-hydraulic feedback networks to counteract the flutter conditions, the eventual integration of the suppression system into an advanced aircraft control system holds promise of extending the aircraft performance with a minimal increase in control hardware.

In order to develop a working suppression system dealing with wing/store flutter and to resolve technical problems in actual systems implementation, an active flutter suppression system was designed and incorporated into a 30% scale model of the YF-17 aircraft. The model has a leading edge and a trailing edge control surface. A store configuration was intentionally designed that featured a violent flutter condition. In the series of wind tunnel tests performed in 1977, a feedback control system, consisting of a number of filters and a simple gain, phase shift circuit was able to suppress violent flutter conditions. For instance, at M = 0.60, the projected improvement in the flutter dynamic pressure was 29%. The analytical and test results related to the test sequence are documented in an AGARD report (Reference 1).

The experience gained in the above-mentioned wind tunnel tests pointed the way to further improvements that could be made in the flutter suppression system and the test apparatus: 1) Augmenting and upgrading the mechanical and electrical components, 2) designing more complex control laws with the goal of a demonstrated improvement of 70% in the flutter dynamic pressure, and 3) using the Hewlett-Packard 5451C Fourier Analyzer to monitor the control law performance and to point out ways they can be improved.

In order to concentrate the new test effort on flutter control law development and suppression system performance, a single test configuration was selected which featured the above-mentioned severe flutter condition. In addition to Northrop-developed control laws, three control laws were supplied by European countries at the invitation of the U.S. Air Force. The international contributors were British Aerospace, MBB, and ONERA. These control laws were interpreted, mechanized and integrated into the flutter suppression electronics console at Northrop's Hawthorne facility prior to test entry.

The wind tunnel tests were performed in September-October 1979 at the NASA Langley Center Sixteen-Foot Transonic Dynamics Tunnel. In addition to Northrop and AFFDL personnel, all European participants were on-site to witness the tests and to suggest modifications to their control laws, as the need arose. This paper describes the major features of the improved flutter suppression model, the test monitoring techniques, and the analytical and experimental results of the newly-developed control laws. The control laws developed by the European participants are presented separately by their originators.

THE REFURBISHED MODEL AND NEW INSTRUMENTATION FEATURES

The flutter suppression model is a 30% scale half span model mounted on a set of roll bars and stabilized with forward and aft tension cables. Leading edge and trailing edge control surfaces are operated by miniaturized hydraulic actuators. A detailed arrangement of the model is shown in Figure 1 with additional information on the model given in References 1, 2.

The basic configuration adopted in the present test sequence is Configuration B of the previous test sequence. It features an empty tip launcher rail and an AIM-7S missile attached to a pylon near the wing tip (W.S. 60.75). As part of the refurbishing work, the leading edge and trailing edge surface hinge mechanisms were completely redesigned to improve their ruggedness. The original angular potentiometers attached to the hinges were replaced with rotary variable differential transformers (RVTD's). The new design with

RVDT's achieved a more reliable surface position sensing. It also featured new surface-to-actuator-shaft attachments for improved reliability and interchangeability.

Four (4) Sundstrand accelerometers were installed in the wing sections to serve as the sensors for flutter suppression. The sensors, identified as a_1 through a_4, were installed in the following locations:

Accelerometer No. 1 (a_1)	W.S. 51.45	F.S. 145.18	(25%c)
Accelerometer No. 2 (a_2)	W.S. 51.45	F.S. 158.00	(76%c)
Accelerometer No. 3 (a_3)	W.S. 60.75	F.S. 148.56	(25%c)
Accelerometer No. 4 (a_4)	W.S. 60.75	F.S. 157.47	(70%c)

The approximate locations of these sensors are indicated in Figure 1. Additional model instrumentation included wing and horizontal tail moment strain gages, the control surface servo inputs, and the angular position potentiometers mentioned above. For the new test sequence, additional wiring and tubing were installed to accommodate the wing and tail moment gage bridges and the instrumentation of the AIM-7S store functioning as the flutter stopper.

The control console panel was modified to accommodate additional required controls and indicators. The existing patch boards were reorganized and the control console was rewired to accommodate new control laws developed at Northrop and by European country participants. Additionally, in order to improve the actuator response, a new hydraulic power unit was acquired to supply fluid at the rate of 1.6 gallons per minute at a pressure of 2000 psi.

Remote control of the hydraulic power unit was added to the console to provide for start/stop and bypass control of this unit from the wind tunnel control room.

THE FLUTTER DETECTOR AND THE FLUTTER STOPPER

Two pieces of hardware were added to the flutter suppression system in order to protect the model in case of an unexpected flutter occurrence. The first of these was a flutter detector which was designed to indicate when a flutter condition existed, while the second device was a "flutter stopper" which featured a mass inside the AIM-7S store that could be fired ahead rapidly to interrupt the flutter condition once it was identified by the flutter detector. Separate bays in the control console monitored and controlled the performance of the flutter detector and the flutter stopper.

The flutter detector has a number of electronic circuits which sense when the amplitude of the input signals from the model are equal to or above a preset level. A digital counter counts the number of pulses detected. A triggering signal is generated when a preset number of pulses are accumulated by the detector. To prevent false triggering due to spurious noise signals, the pulse counter is reset to zero if a certain time lapse occurs between consecutive pulses. In wind tunnel tests, when the trigger conditions are met, the triggering signal may be applied to activate the flutter stopper and to operate the tunnel flow bypass valves. Figure 2 is a block diagram showing the basic operation of the flutter detector. Figure 3 is the oscillograph record of a number of the responses of the YF-17 model instruments acquired in the wind tunnel when a moderate flutter condition was encountered. The time traces read from left to right, with all transducers and scales identified at the left side of the figure. The top trace of the figure shows the trigger signal, which appeared only after the wing bending and torsion bridge gages experienced a number of high stress cycles. Prior to that time, the stress cycles with a moderate amplitude were ignored by the flutter detector.

A scale model of the AIM-7S Sparrow store was designed to function as the flutter stopper. The new store featured a spring-loaded movable mass (weight = 3 pounds). In the normal latched position, the store model has the same c.g. location and mass inertia in pitch and yaw as the store used in the previous tests (Reference 1). In case of severe flutter, the mass can be released by a solenoid mechanism, which allows the mass to move forward inside the store housing for a maximum distance of 10 inches in approximately ¼ second. The store with the changed c.g. location was designed to disrupt and stop the flutter condition of Configuration B. When the movable mass is in the forward position, it can be reset remotely to any desired latched position along the 10-inch travel distance. The reset is executed through the operation of a gear motor and ball-nut assembly. A linear potentiometer with a contact point on the movable mass indicates the instantaneous mass location inside the flutter stopper. A sectional drawing showing the flutter stopper/guide rail assembly is given in Figure 4. Figure 5 shows the details of the assembly inside the store.

Flutter analyses of the model were performed when the mass was in the normal and deployed positions. Figure 6 shows the results of these analyses. It indicates that the flutter stopper can increase the model flutter speed quite significantly. Two different curves are shown for the deployed result. In one, the analysis was performed without any modification to the analytical data, while in the other, the bending and torsion frequencies for the system with the mass deployed were acquired in a ground vibration test and input to override the analytically-obtained frequencies. It is seen that the increase in flutter speed with the measured frequencies is less beneficial than with the purely analytical result. Nevertheless, both results provide for a satisfactory pressure margin in flutter dynamics. The effectiveness of the flutter stopper was later confirmed in the wind tunnel entry.

NORTHROP CONTROL LAW DEFINITION AND ANALYSIS

In order to establish accurate open loop aircraft transfer functions as a basis for new control law development and to make use of the previous wind tunnel test data, a new flutter analysis was performed on the YF-17 flutter suppression model. Simultaneously, a ground vibration test was performed at the Hawthorne facility. During the test, the tunnel supporting system used for the YF-17 model was duplicated to the extent possible. Table 1 presents a comparison among the natural vibration frequencies measured

previously in the ground vibration tests at Wright-Patterson Air Force Base and at the Hawthorne facility, and those computed in the present analysis. This analysis differs slightly from the final analysis presented in Appendix A of Reference 1 in that the stiffnesses used in that analysis had been arbitrarily reduced slightly in order to match the test results. It is seen that the present analysis shows a reasonable correlation with the test results.

TABLE 1. NATURAL VIBRATION FREQUENCIES (IN Hz) OBTAINED IN THE GROUND VIBRATION TESTS COMPARED WITH ANALYTICAL RESULTS, CONFIGURATION B.

MODE	AFFDL GVT	HAWTHORNE GVT	TUNNEL GVT	ANALYSIS
1	4.80	4.44	4.40	4.63
2	7.40	7.10	7.40	7.19
3	12.80	12.31	12.20	13.40
4	14.20	14.23	14.00	14.88
5	19.00	18.66	19.40	19.14

A study was performed to determine the level of refinement necessary in the wing paneling for unsteady aerodynamic forces in order to obtain a converged solution. Special attention was given to the proper paneling of the two control surfaces used in flutter suppression. Based on this study, a panel scheme using 195 boxes on the wing surface was selected for the analysis. The new analysis for Configuration B resulted in a matched point dynamic pressure of 84 psf at M = 0.80 (see Figure 6). The flutter frequency at the match point is 6.0 Hz.

Once confidence in the open loop analysis had been attained, the construction of new control laws could proceed. Figure 7 is a representative block diagram of the new control laws. In the figure, θ_{01} and θ_{02} are two model response outputs (e.g., the angular and vertical accelerations derived from the outboard sensor pair) which are filtered, blended and then fed back to one of the control surfaces. G_1 and G_2 are aircraft transfer functions that related model response to the command to the control surface actuators. The η terms represent response to noise sources, primarily the tunnel turbulence. The F_i terms are pseudo-integrators which convert the accelerometer outputs to responses which approximate velocity and displacement signals. The "pseudo" designation is used because the integrators are of the form 1/(s+a) where "a" is a constant used to prevent steady state drift. The R_i components are gain settings which control the relative amplitudes of the velocity and displacement signals, with the R_5 term controlling the overall gain. The H block is a series of filters which act together as a bandpass to limit the amount of signal which is fed back at frequencies removed from the flutter frequency.

A synthesis procedure (Reference 3) was applied to determine the constants R_1 through R_4. Altogether, four control laws were organized by Northrop and tested in the wind tunnel. They are identified as control laws N1, N3, N3T and N3P. The control surfaces and the accelerometers used by each of these control laws and the control laws contributed by the European countries are identified in Table 2.

TABLE 2. CONTROL LAWS FOR THE FLUTTER SUPPRESSION MODEL

CONTROL LAW	RESPONSIBLE ORGANIZATION	CONTROL SURFACE		ACCELEROMETERS			
		LEADING EDGE	TRAILING EDGE	a_1	a_2	a_3	a_4
N1	Northrop	X				X	X
N3	"	X		X		X	X
N3T	"		X	X		X	X
N3P	"	X	X	X		X	X
BAE	British Aerospace	X				X	X
MBB	Messerschmitt-Bolkow-Blohm		X	X	X	X	
ON	ONERA	X					X

The block diagrams of the four Northrop control laws are shown in Figures 8 through 11.

Pretest analyses were performed on all Northrop control laws, with some additional analyses made at Hawthorne while the test was in progress at the NASA Langley TDT facility. Figures 12 through 15 present analytical data for the four Northrop control laws. Figure 12 is a plot of the stability behavior of the open loop system and of Control Law N1 at M = 0.80 using dynamic pressure Q as a parameter. The data were acquired by the characteristic diagram method. Figures 13 a, b are the open loop Nyquist plots of Control

Law N3 at two dynamic pressures. Based on Nyquist data of this type, the system gain and phase margins were established as a function of the dynamic pressure. Figures 14 a, b are similar open loop Nyquist plots for Control Law N3T. The data indicated the N3T Control Law was substantially less effective than Law N3. This point was confirmed in the wind tunnel tests and is discussed later in the paper. Control Law N3P used both the leading and trailing edge control surfaces and is simply a superposition of the N3 and N3T control laws. The stability plot of this law, based on the characteristic diagrams method, is shown in Figure 15.

CONTRIBUTED CONTROL LAWS

As mentioned in the previous section, three (3) control laws were contributed by three separate European country participants: The British Aerospace Corporation, MBB and ONERA. The control laws are identified by the letters BAE, MBB and ON, respectively (see Table 2). The block diagrams representing the three control laws are given in Figure 16 through 18. As can be readily observed, even though they were designed to suppress a single flutter condition, the control laws feature a great diversity in their basic organizations and in the transducers and control surface(s) they used.

TEST MONITORING TECHNIQUES

An important aspect of the project was the development of procedures that monitored and directed the wind tunnel test program. Prior to the test entry, monitoring programs were developed on the Hewlett-Packard 5451C Fourier Analyzer. Actual servo hardware and an analog simulation of the YF-17 model were used to try out and debug the monitoring programs. In this section, some key monitoring programs used in the tunnel entry are described.

Nyquist Plot

A key monitoring program was developed to extract the open loop transfer function of the aircraft flutter suppression system when the control loop was closed. The following sketch defines the terminology that is used in the discussion.

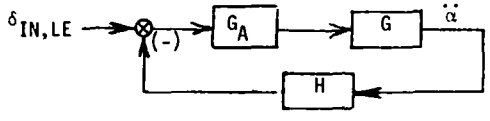

where

G_A = actuator and servo transfer function

G = open loop transfer function of the aircraft

H = transfer function of the feedback loop

A further term is G_c = the closed loop transfer function:

$$G_c = \frac{G_A G}{1 + G_A G H} \tag{1}$$

The Nyquist criterion required a plot of $G_A GH$. The assumption for developing the test monitoring technique was that it should be possible to make a relatively accurate measurement of G_c but that a direct measurement of G would be difficult since it would require the measurement of a mode that was suppressed and because noise would contaminate a measurement made inside the loop. The alternative was to extract G from the measured values of G_c, G_A and H. (The latter two transfer functions could be measured very well with the loop open.) The open loop transfer function was then obtained from Equation 1:

$$G = \frac{G_c}{G_A (1 - G_c H)} \tag{2}$$

The Nyquist diagram could then be calculated directly.

The above example illustrates the case involving a single feedback signal. For a multiple sensor system, reference is made to a typical flutter suppression control law as shown in Figure 7. In the figure, the F_i's and H are compensation filters, while the R_i's are potentiometer settings. In this case, the measurements are made of G_{1c} and G_{2c}, which are θ_{01}/δ_c and θ_{02}/δ_c, respectively. The open loop transfer functions G_1 and G_2 are then:

$$G_1 = \frac{G_{1c}}{1 - R_5 H \left[G_{1c} (R_1 F_1 + R_2 F_2) + G_{2c} (R_3 F_3 + R_4 F_4)\right]} \tag{3}$$

$$G_2 = \frac{G_{2,c}}{1 - R_5 H \left[G_{1c} (R_1 F_1 + R_2 F_2) + G_{2c} (R_3 F_3 + R_4 F_4)\right]} \tag{4}$$

Once the open loop transfer functions have been computed, it is possible to construct the open loop Nyquist plot. The formula for the Nyquist function is:

$$N = R_5 H \left[G_1 (R_1 F_1 + R_2 F_2) + G_2 (R_3 F_3 + R_4 F_4)\right] \tag{5}$$

The application of the Nyquist plot technique in actual wind tunnel test will be illustrated later in the section dealing with Experimental Results.

The measurement of the closed loop transfer functions required that some type of excitation be applied at the δ_c point of Figure 7. During the simulation work carried out at Hawthorne, as well as during the later wind tunnel test, the excitation utilized was a random transient that was generated by the Fourier Analyzer. This was a random noise signal that was set to zero in the last 25 percent of the sample period. This made the response to the excitation die out in the sample period (i.e., it was periodic in the "window") and fast Fourier transform techniques were valid. Four thousand samples were taken for every sample period at a rate of 200 samples/sec. for a total of 20 seconds per period. The maximum frequency measured with this setup was 100 Hz. The number of averages used varied depending on the number required to give an adequate signal to noise response. In later wind tunnel tests, a minimum of six (6) ensemble averages were used.

Smoothing of Transfer Functions

Another test monitoring program dealt with the smoothing of frequency domain signals such as aircraft transfer functions. Because of the substantial level of turbulence in the tunnel, the response signal to noise ratios are such that key modal information may be masked by the superimposed noise. In order to reduce the noise effect, smoothing techniques were applied to the measured or processed transfer functions. Methods of smoothing entail performing a Fourier transform on the transfer function to obtain the impluse response of the system. It is assumed that all the response after a certain time in this record is uncorrelated with the input excitation. A simple means of removing this repsonse is to apply a rectangular window to the impulse response that zeroes out all response after a certain time.

When this truncated response is transformed back to the frequency domain, the resulting transfer function is considerably cleaner, but retains all the key modal information.

A criticism of this "rectangular" window is that it creates a high frequency signal that is superimposed on the transfer function. This behavior can be eliminated if a different type of window, the exponential window, is applied to the impulse response.

A drawback of an exponential window is that it affects the estimated damping. Reference 4 shows that if this window is applied to a single degree of freedom transfer function, the damping is modified according to the formula:

$$c'/c_0 = c/c_0 + \frac{\alpha'}{\omega_n} \qquad (6)$$

Where c'/c_0 is the damping obtained from the smoothed transfer function, c/c_0 is the actual damping, α' is the decay constant in the exponential window and ω_n is the natural frequency of interest. If the window is applied n times, the correction term is also increased by a factor of 'n'. Although this does not appear to be a major correction, it was decided to avoid this complication and use the rectangular window.

Peak-Hold Damping Trend

The peak-hold spectrum method provides Fourier transformed measurements of the model responses, filtered through 250 narrow-band circuits. The peak response within each interval is registered on a screen until the peak amplitudes are stabilized. The damping of a resonant mode is proportional to the inverse of the peak amplitude at that mode frequency. The damping trend data can be extrapolated as the dynamic pressure Q is increased to determine the projected flutter dynamic pressure for either a controlled or uncontrolled system. Because of the simplicity of the approach in that knowledge of the excitation is not required, the method was used extensively in the tunnel test to determine the control system effectiveness and, with the assistance of other monitoring programs, to revise the tunnel test strategy.

Other monitoring programs developed for the wind tunnel tests included the determination of new feedback constants to cause a moderate phase shift of the feedback signal, and an optimization program to improve the control signal while the test was in progress. Additionally, open and closed loop transfer function acquisition, as well as other processing techniques, were applied to the real time data recorded on a 14 channel FM tape system. A substantial portion of the results presented in the following section was generated from the FM tape data.

EXPERIMENTAL RESULTS

Peak-Hold Damping Data

After setting up the flutter suppression model in the NASA Langley TDT facility and performing a simple ground vibration test, actual wind-on tests were initiated in early October and lasted 15 working days. Altogether, 27 runs were made consisting of 511 test points. The key results for the uncontrolled flutter model and for the model with various control laws are summarized in Figures 19 through 26 in the form of peak-hold damping trend plots. The plots were based on the signals from the wing torsion moment strain gage.

Referring to Figure 19, the damping trend indicated a projected open loop flutter dynamic pressure of 75 psf. This result was confirmed by two other methods. One method was based on the Nyquist criteria using open loop data extracted from the closed loop transfer functions as explained in the previous section on Test Monitoring Technqiues. The other was the Royal Aircraft Establishment (RAE) method based on the extrapolation of the two natural modes in flutter. Experimental results throughout the test period showed a consistent flutter dynamic pressure of 75 psf. Post processing with the HP modal analysis indicated a flutter dynamic pressure of 74 psf. This was in contrast to the predicted analytical result of

84 psf, and the experimental results of 83.5 psf acquired in 1977. It is difficult to determine the precise cause of the deviation in the flutter dynamic pressures. The most probable cause was that the model dynamic behavior was sensitive to the constraints on the half fuselage. The constraints were caused by the supporting system which was somewhat redundant. Any slight misalignment could influence the natural frequency modes in a subtle manner, which in turn could affect the flutter dynamic pressure. Another factor which could affect the analytical results were the deviations in physical data of the AIM-7S Store. After test, slight deviations were discovered of the new store mass, c.g. and pitch inertia properties. Using the corrected data, the flutter dynamic pressure was dropped from 84 psf to 80 psf. During the test entry, because of test time limitations, and in view of the consistent experimental results, it was decided to bypass this problem and to use a dynamic pressure ratio, (Q/Q_f), for evaluation purpose when analytical and experimental data were compared.

Figures 20 through 26 show that all the control laws were effective in suppressing the flutter condition. On the figures, the symbols indicate actual data points while the straight lines are projections obtained from a linear regression of the data points.

RMS Response Data

The FM tape data was processed to calculate power spectra information for the majority of the test points where peak hold information was taken. The purpose of this analysis was to provide a more quantitative comparison of the various control laws. It also provides insight into the model behavior and into subjective criteria that were used to guide the conduct of the test.

For the leading edge control laws, Table 3 presents RMS values for the leading edge control surface position and the wing root bending and torsion strain gage data. The results are presented in two frequency ranges, allowing for the distinction between the lower frequency response associated with the open loop flutter mode and those responses associated with higher frequencies. The first row in Table 3 gives the responses at the highest open loop dynamic pressure at which the model was tested. A careful examination of the data in this table reveals some of the subtleties of the various control laws. For instance, it is seen that the N1 and the BAE control laws did a better job of suppressing the flutter mode than the N3 law, but that the N3 law had considerably less response in the 10-20 Hz range than the aforementioned laws. Figures 27-29 give the power spectral responses of the leading edge surface position for the three control laws and make this point even more clearly. A final point from Table 3 is that the open loop response of Test Point 64 is quite high and, in fact, indicates that this was not a prudent condition at which to be testing.

Figures 30 and 31 compare the PSD's of the wing torsion gage for the uncontrolled case of Test Point 64 with the controlled case at a dynamic pressure that is 75% higher. Note that there is 20 db magnitude difference in the scales of the two figures. The uncontrolled PSD is dominated by the response at 6 Hz, while for the controlled case, the 6 Hz mode is suppressed so well that higher frequency modes dominate the response.

TABLE 3. RMS RESPONSE DATA OF THE YF-17 MODEL FOR VARIOUS LEADING EDGE CONTROL LAWS.

CONTROL LAW	Q (PSF)	TEST POINT	LEADING EDGE POSITION (DEGREES)		WING BENDING MOMENT (IN-LBS)		WING TORSION MOMENT (IN-LBS)	
			0-10 Hz	0-20 Hz	0-10 Hz	0-20 Hz	0-10 Hz	0-20 Hz
None	73	64	-	-	41.4	49.8	42.7	44.1
N1	98	97	.52	.86	29.9	51.0	8.3	22.1
N3	101	124	.63	.69	37.6	50.2	11.7	17.7
BAE	105	201	.61	.96	29.9	41.6	8.3	22.6
ON	100	471	.96	.96	62.0	70.1	16.5	22.6
N1	128	104	.70	1.10	41.7	61.0	9.0	28.6
N3	128	127	.87	.97	49.5	66.2	12.5	22.1
BAE	129	211	.71	1.13	37.3	51.5	9.6	27.7

Table 4 shows RMS data for the trailing edge control laws, and the N3P law, which used both control surfaces. The trailing edge laws are seen to have required less control activity, but they were not able to demonstrate as much of an improvement in dynamic pressure as the leading edge laws. Transfer function data tend to indicate that the trailing edge laws were characterized by low phase margins, making them sensitive to small changes in the feedback law or the tunnel condition.

The N3P control law performed well, particularly when it is considered that no attempt was made to improve upon the law during the tunnel test. The leading edge RMS response for this law is given in Table 4 where it is seen to be considerably less than for any of the single surface laws at an equivalent test condition. Figure 32 shows the PSD of this response which, when compared with Figures 27 and 28, shows that the peak amplitudes are much less for the N3P law, although there is response over a broader frequency range.

Unfortunately, trailing edge data was not recorded onto FM tape for the N3P law, but the impression formed during the test was that the trailing edge amplitude was less during the test of the N3P law than it was for any of the trailing edge laws performing alone.

TABLE 4. RMS RESPONSE DATA OF THE FLUTTER SUPPRESSION MODEL FOR VARIOUS TRAILING EDGE CONTROL LAWS AND THE N3P LAW.

CONTROL LAW	Q (PSF)	TEST POINT	CONTROL SURFACE INPUT (DEGREES)		WING BENDING MOMENT (IN-LBS)		WING TORSION MOMENT (IN-LBS)	
			0-10 Hz	0-20 Hz	0-10 Hz	0-20 Hz	0-10 Hz	0-20 Hz
N3T	96	249	.32	.34	28.2	39.0	26.2	29.8
MBB	99	356	.24	.25	45.0	53.0	28.0	30.2
N3P	128	N3P	.52	.66	42.0	59.0	18.0	26.9

A final comment is that the PSD responses measured from the FM tape could have been measured equally well during the wind tunnel test. This would have complemented the peak hold measurements that were used to decide whether the test could proceed to higher dynamic pressures. The HP Fourier Analyzer has considerable flexibility in terms of available displays and calculations it can perform. Data gathered during the test could be stored on disk and recalled for display as needed, thereby centralizing and streamlining the real time data gathering process.

Closed Loop Transfer Function Data of the YF-17 Model

During the wind tunnel tests, model transfer functions were acquired through control surface excitation. The excitation of either the leading edge or the trailing edge control surface was initiated by the random DAC signal from the Hewlett-Packard Fourier Analyzer. The responses were measured by the accelerometers and the wing root section strain gage bridges. The DAC and the response signals were recorded on the FM tape for later processing. Simultaneously, selected transfer functions were created using six ensemble averages of 20 seconds each during the tests and were stored in the Hewlett-Packard System Disc. The transfer functions generated onsite were used to monitor the model behavior, and for a closed loop system, to determine the effectiveness of the control law. To differentiate from the onsite generated transfer functions, the transfer functions generated at Hawthorne based on the FM data (and using the same number of ensemble averages) are called the post-test transfer functions. The transfer functions presented in this section were acquired with Control Law N3P in operation, i.e., the control law using both the leading and trailing edge control surfaces. The responses used in generating the transfer functions were the acceleration differentials $(a_3 - a_1)$, $(a_4 - a_3)$, as well as the wing root section bending moment and torsional moment gages. These data corresponding to Q = 95 psf are presented in Figures 33 through 38. Data in Figures 33 through 36 were generated onsite, while Figures 37 and 38 are data from post-test processing.

Referring to the figures, the major response peaks below 20 Hz were higher using the trailing edge surface than with the leading edge surface (by a factor of two or more). The difference is most prominent for transfer functions involving $(a_3 - a_1)$. (Compare Figures 33, 35.) Also, the phasing signal is substantially noisier when leading edge excitations are used.

The effect of increasing dynamic pressure Q for the same transfer function, is that the peak amplitudes vary approximately with the dynamic pressure. (Data not presented in this paper.) For a set of transfer functions, the changes of the phase signal corresponding to moderate Q changes (from 72 to 95 psf) were barely noticeable.

An examination of the transfer functions for the wing bending moment and torsional moment gages reveals generally similar patterns for both, some mixing of the actual bending and torsional signals by the strain gage bridges. As to be expected, the modal peaks in the 12-15 Hz range, corresponding to the pylon-yaw/wing-bending mode, and the tail surface bending mode, were more prominent for the transfer functions of the bending moment gage. (See Figure 37.)

Extraction of Open Loop Response

The need to smooth the measured model transfer functions prior to other processing was discussed previously. The noisiness of the transfer functions may be evidenced in the data presented in Figures 33 through 38. This subsection illustrates the extraction of the open loop transfer functions from the closed loop transfer functions after they are smoothed through the use of the rectangular filters.

Closed loop transfer functions were acquired for Test Point 504 at M = 0.80, Q = 95 psf, with Control Law N3 in force. After smoothing, the results are given in Figures 39, 40. In order to extract the open loop transfer functions for Nyquist criteria analysis, it is necessary to establish the feedback functions $F_iH(i = 1,4)$ as shown in the block diagram of Figure 7. The four functions are presented in Figure 41, while the R_i parameters for this case are, respectively, 0.365, 0.116, 0.351, 0.837 and 0.750. Figures 42 and 43 show two open loop transfer functions that result when all these data are entered into Equations 3 and 4.

With the open loop transfer functions, it is possible to construct the open loop Nyquist plot from which, for the case of a single control surface, the system gain and phase margins can be readily determined. The Nyquist function is generated according to Equation (5). For the case described above (Figures 39-43), the resulting Nyquist plot is shown in Figure 44. It is seen that the plot has the desirable encirclement around the -1 point, indicating Control Law N3 at this test condition has large gain and phase margins.

During the wind tunnel test, a number of Nyquist plots were acquired in the above described manner. They were valuable in determining the margins of the control system, as well as in defining ways of improving control laws.

Determination of System Frequencies and Dampings

The previous sub-sections describe how the measured transfer function data are prepared for identification of the system frequency and damping parameters. The HP Fourier Analyzer has a modal analysis package (Reference 5) that is well suited for the identification task. One drawback of that system is that it cannot identify modes that are negatively damped. Hewlett Packard has provided Northrop with a modified version of the system that does have a capability for identifying unstable modes.

Another complicating factor in the identification process is that, near the flutter point, there are two lightly damped modes that are very close in frequency. This can confuse the identification system, with significant user interaction required to obtain satisfactory results. With these qualifications, Figure 45 shows open loop frequency and damping estimates from the data gathered during Run #27 of the tunnel test. Only the two lowest frequency modes, which represent most of the total flutter mechanism, are shown. The dynamic pressure range is limited by the range over which it was prudent to excite the model. The flutter Q is 74 psf for this case with a rapid crossing of the stability boundary.

Figure 46 compares the open loop result with those obtained when Control Law N3 (see Table 2) was used. It is seen that over the range measured, the system remains very stable and in fact it is impossible to project a closed loop flutter speed. The comparison of the open and closed loop frequencies shows that the modes remain well separated when the control law is in force.

Figure 47 shows a similar comparison for Control Law N3T, a trailing edge law. No closed loop data are available for this control law above 80 psf, but the implication is that while this system is still stable, it does not perform as well as the N3 law.

Finally, Figure 48 shows the results when the N3 and N3T laws are engaged simultaneously. This is designated the N3P law, and it is seen that this law gives the best stability characteristics. In fact the modal damping is so high that identification is considerably less precise for this case.

COMPARISON OF ANALYTICAL AND EMPIRICAL TRANSFER FUNCTIONS

The development of the control laws relied upon the analytically derived transfer functions that relate the accelerometer responses to the control surface inputs. It is of interest, therefore, to see how closely transfer functions measured in the tunnel compare with the analytical ones. A confounding factor is that the measured open loop flutter dynamic pressure was approximately 12% lower than the predicted flutter dynamic pressure, a fact mentioned previously in the paper. The results given below are, therefore, presented as a function of Q/Q_f, where Q is the dynamic pressure at which the transfer function is presented and Q_f is the open loop flutter dynamic pressure (predicted or measured, depending on the context).

Figures 49, 50 present the comparison between the measured and analytical open loop transfer functions of the $(a_3 - a_1)$ response due to the leading edge input. The comparison was made at a (Q/Q_f) ratio of approximately 1.30. The experimental open loop data were extracted from the closed loop transfer function data acquired at Test Point 504 when Control Law N3 was applied. The plots are in polar form, allowing a simultaneous comparison of magnitude and phase information. The numbers on the figure correspond to frequencies in Hertz. It is seen that there is a good agreement between the two plots in both magnitude and phase. When one considers that the magnitude and phase information is influenced by mass, stiffness, aerodynamic and control surface factors, the comparison is all the more impressive. The agreement appears to deteriorate as the frequency increases, but a qualitative resemblance remains.

Figures 51, 52 show a similar comparison for the $(a_4 - a_3)$ response due to the leading edge control surface input. The comparison is seen to be very good for the lower frequency modes but the higher modes have a measured phase that is 90^o ahead of the analytically predicted phase. The magnitudes are seen to compare quite well.

The preceding four figures dealt with responses to the leading edge control surface. If responses to the trailing edge control are examined, the comparison between analytical and empirical results is not as good. Figures 53, 54 make this comparison for $(a_3 - a_1)$ under trailing edge excitation at $Q/Q_f = 1.07$. For this transfer function, the measured phase of the flutter mode is approximately 45^o ahead of the analytical one. The higher modes differ considerably in magnitude. The analytical mode at 17 Hz does not appear in the experimental result because the higher modes have been removed for the sake of clarity.

The comparisons presented here serve to explain a number of events that occurred during the course of the tunnel test. The most significant observation is that the close agreement between the analytical and the measured results for the leading edge case explains why the leading edge laws performed as well as they did. During the test, the only changes that were required in the analytically derived control laws were increases in the overall gain levels by small amounts.

The empirical data also explains why the N1 and BAE control laws had difficulty with a 13 Hz mode. The indication is that the analytical phase information for this mode was in error to the extent that these control laws were driving this mode. Further study is required to determine why the N3 law did not have this difficulty.

The primary conclusion from the trailing edge data is that there are significant discrepancies between the measured and analytical results. The least squares synthesis procedure was applied during the test program to modify the analytically derived N3T law, with the altered control law showing some improvement.

Both the analytical and the experimental data indicate why there has been difficulty in making the trailing edge surface an effective controller. At a dynamic pressure which is 7 percent above the open loop flutter speed, Figures 53, 54 show that there is a relatively small phase range in the flutter loop. Additional investigation shows this situation worsens as the dynamic pressure increases, and that there may be problems with higher modes.

Detailed examination of the trailing edge data indicates that the inability to accurately predict the analytical response, coupled with the apparently non-optimal sensor selection, combined to make trailing edge control difficult. This is unfortunate since the tunnel tests indicated that this surface is quite powerful in the sense that it creates strong responses for relatively small surface motions. However, based on the experiences gained in the wind tunnel entry, it is now possible to organize new sensor combinations, or to define a new trailing edge surface, for the purpose of implementing trailing edge control laws and achieving effective flutter suppression.

CONCLUSIONS

Aircraft active wing/store flutter suppression has drawn substantial interest in the technical community dealing with aeroelastic problems. In concentrating on one severe flutter condition of the fighter aircraft model, it was possible to draw on the talents from two continents to organize control laws and test them in one facility. The differences in background and flutter control philosophy of the contributors are clearly reflected in the diversified control laws submitted for experimentation. It is, therefore, all the more gratifying that in the final test, all the control laws succeeded in serving their intended functions as visualized by their originators.

The wind tunnel test demonstrated a number of milestones which are listed below:

- Applying a number of control laws to a severe flutter condition at M = 0.80, the model was tested at Q/Q_f = 1.70, indicating a flutter speed improvement of approximately 30%. For one control law, a peak-hold damping prediction, substantiated by other appraisals of the test data, indicated a potential for the control law to reach a dynamic pressure 131% above the open loop flutter dynamic pressure.
- The ability to switch from one control law to another at Q/Q_f = 1.40 was demonstrated. This feature is significant in future adaptive flutter control, where control law changes at supercritical speeds are necessary.
- The ability to switch from a leading edge control law to a trailing edge control law, and vice versa, was also demonstrated.
- Test monitoring programs were developed to closely monitor the flutter control system behavior in the wind tunnel. Using the programs, a control law was monitored and improved by a moderate amount at the test site. Phase adjustments were accomplished by changing the control law constants, paving the way for future mechanization of control laws using digital computers.

As described in the paper, post analysis of the test data indicated additional potential for the flutter suppression system, as well as shortcomings which can be corrected in the future. For instance, the trailing edge control laws may be improved through sensor location optimization to expand the phase margins. The control law using two surfaces yielded experimental data which may be applied to investigate the unsteady aerodynamic intercoupling effect, etc. Additional processing of the test data will be continued and reported.

The consistent performance of the active flutter suppression systems reinforces our confidence in the approach. Another technical step ahead involves the development of adaptive control laws for flutter suppression. The adaptive system is needed to deal with the varying wing/store configurations, or flight conditions, or both. With the advancement in digital computers and integrated aircraft control system, and through the concerted effort of the technical community, it is our vision that working flutter suppression systems will eventually be incorporated in modern combat aircraft.

REFERENCES

1. Hwang, C., Winther, B.A., Noll, T.E., Farmer, M.G., "Demonstration of Aircraft Wing/Store Flutter Suppression Systems," AGARD Report R-668, July, 1978.

2. Hwang, C., Winther, B.A., Mills, G.R., "Demonstration of Active Wing/Store Flutter Suppression Systems," AFFDL Report TR-78-65, June 1978.

3. Johnson, E.H., "Flutter Control Law Definition Via Least Square Synthesis," to be Presented in AIAA 21st Structures, Structural Dynamics and Materials Conference, Seattle, Washington, May 1980.

4. Jennings, W.P., Olsen, N.L., Walter, M.J., "Transient Excitation and Data Processing Techniques Employing the Fast Fourier Transform for Aeroelastic Testing," NASA Symposium on Flutter Testing Techniques, pp. 77-114, October 1975.

5. "Modal Analysis Operating and Service Manual," Hewlett Packard Manual No. 05451-90461, March 1978.

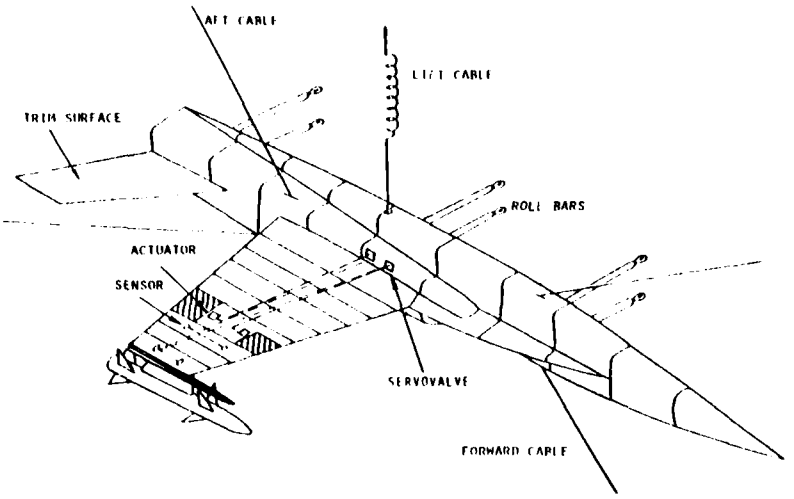

Figure 1. YF-17 Wing/Store Flutter Suppression Model, Configuration B.

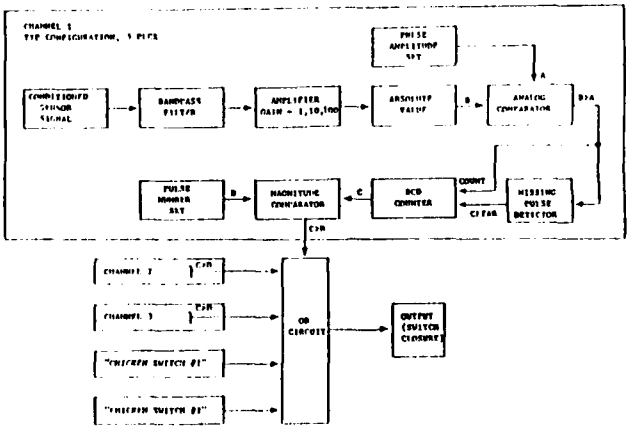

Figure 2. Block Diagram of the Flutter Detector.

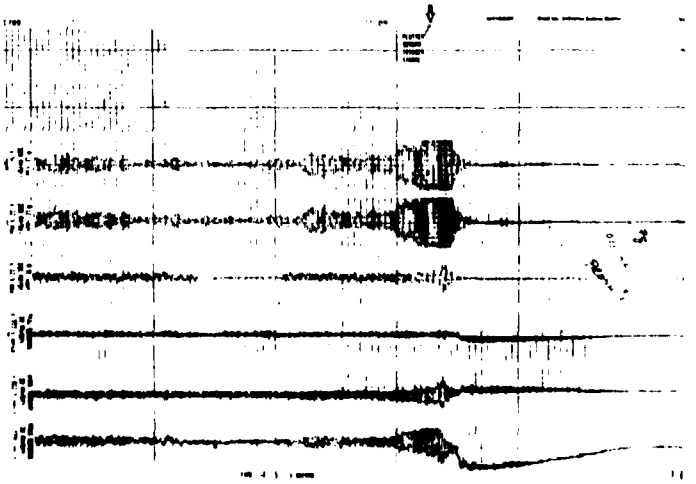

Figure 3. Oscillographs of the YF-17 Model Transducers When a Moderate Flutter Condition Was Encountered. From Top to Bottom, the Six Data Traces Are: Leading Edge Servo Input, Leading Edge Surface Response, Trailing Edge Surface Response, Tail Surface Root Section Bending, Wing Root Section Torsion, and Wing Root Section Bending.

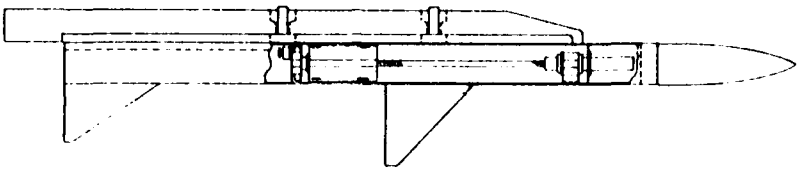

Figure 4. The Flutter Stopper Assembly in the Sparrow Missile.

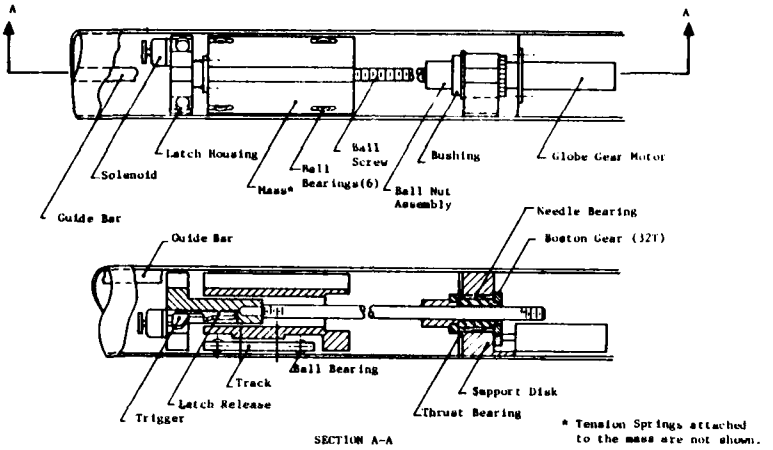

Figure 5. Details of the Flutter Stopper Assembly.

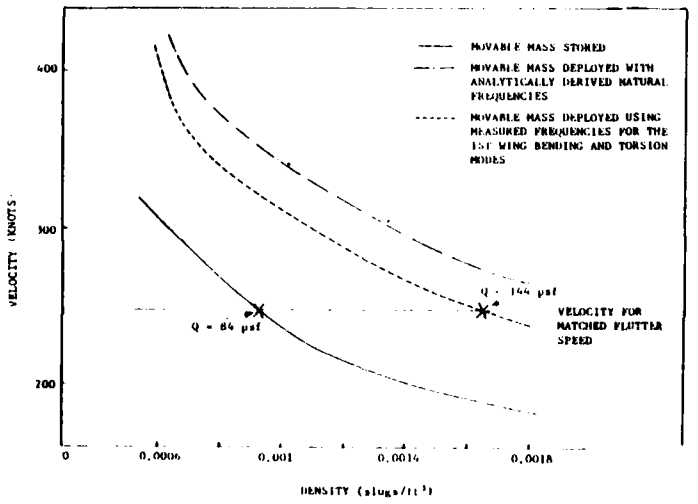

Figure 6. Matched Velocity Flutter Calculations, Configuration B, M = 0.8 for the Flutter Stopper Inactive and Active.

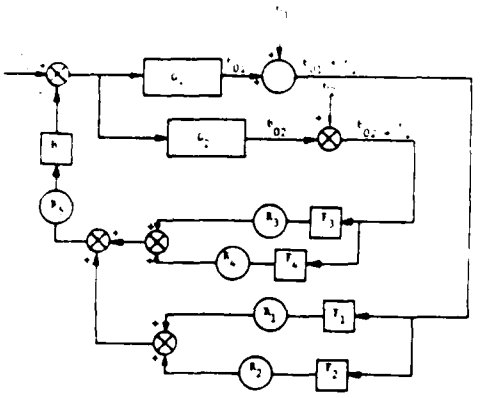

Figure 7. Representative Block Diagram for a Control Law Used During the Tunnel Test.

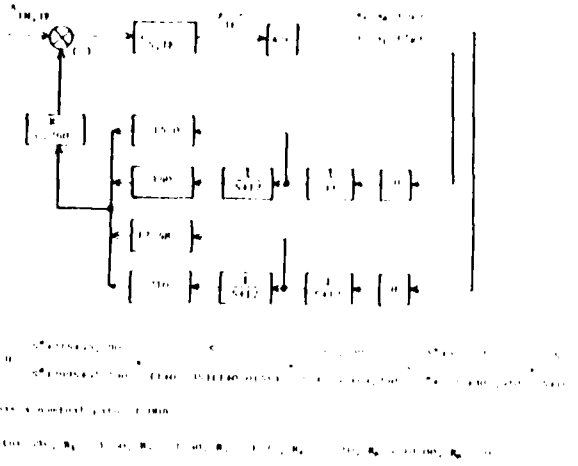

Figure 10. The Trailing Edge Surface Control Law (N3T).

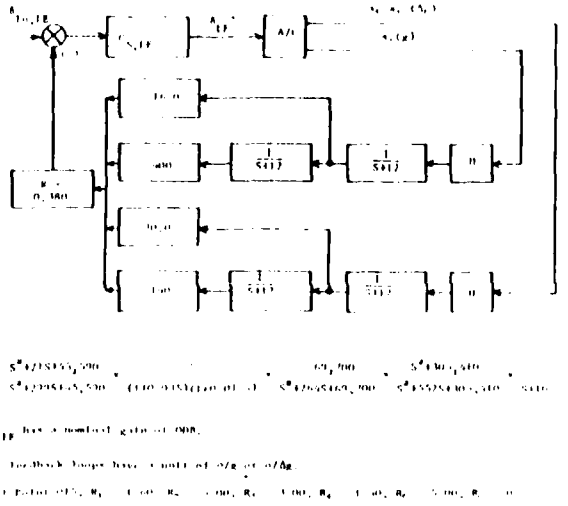

Figure 8. The Leading Edge Surface Control Law (N1).

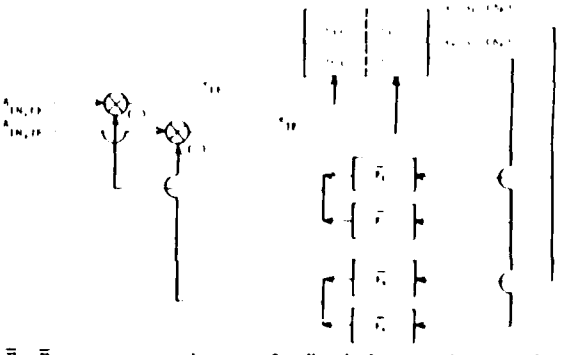

$\bar{F}_1, \bar{F}_2$ represent the two feedback loops of Control Law (N3), with the K block included.
$\bar{F}_3, \bar{F}_4$ represent the two feedback loops of Control Law (N3T), with the K block included.
The G_{ij} elements are the aircraft/servo transfer functions, i = transducer index, j = servo signal index. Test Point 487.

Figure 11. The Two Surface Control Law (N3P).

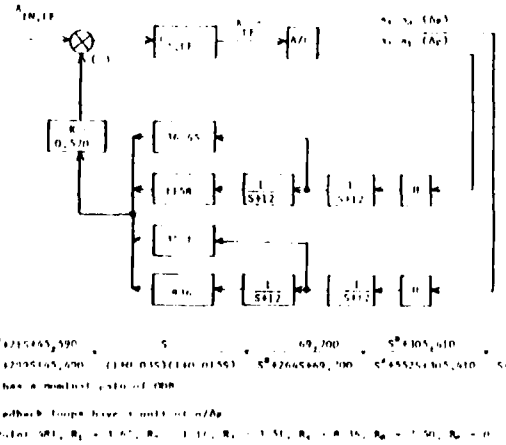

Figure 9. The Three Transducer Control Law (N3).

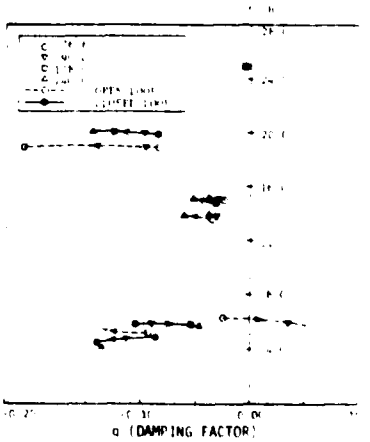

Figure 12. Characteristic Diagram Results of the YF-17 Model With and Without the Leading Edge Surface Control Law N1, K = 0.75.

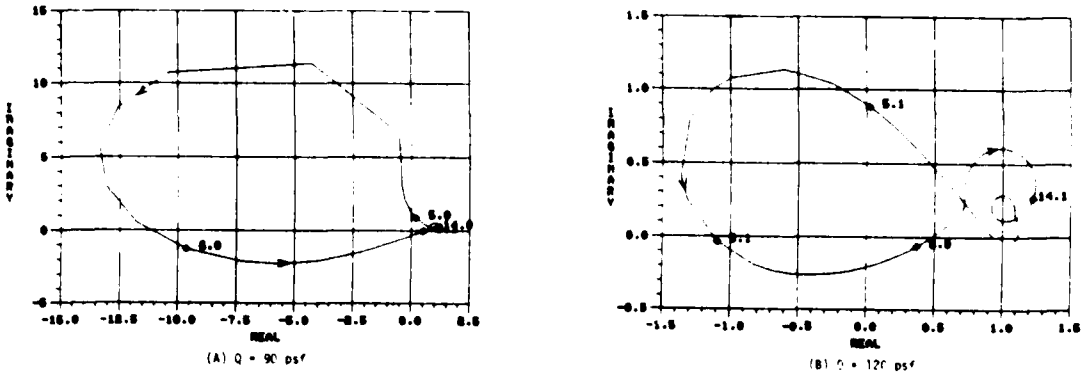

(A) (B)

Figure 13. Open Loop Nyquist Plots of the YF-17 Model With Control Law (N3), K = 0.75.

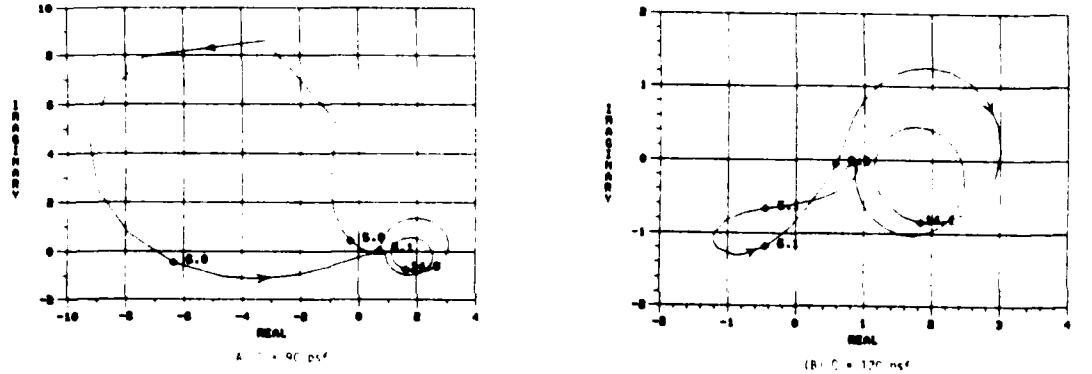

(A) (B)

Figure 14. Open Loop Nyquist Plots of the YF-17 Model With Control Law (N3T), K = 1.00.

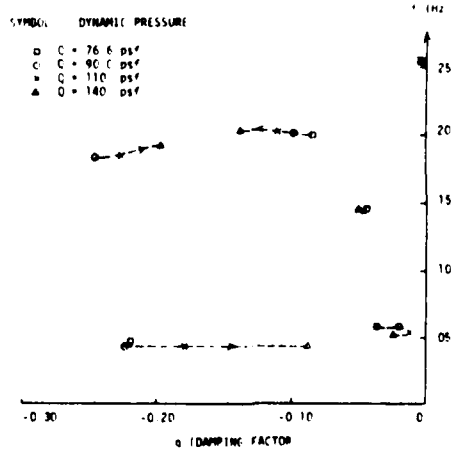

Figure 15. Characteristic Diagram Results of the YF-17 Model With the Two Surface Control Law (N3P). M = 0.80, K_{LE} = 0.75, K_{TE} = 1.00.

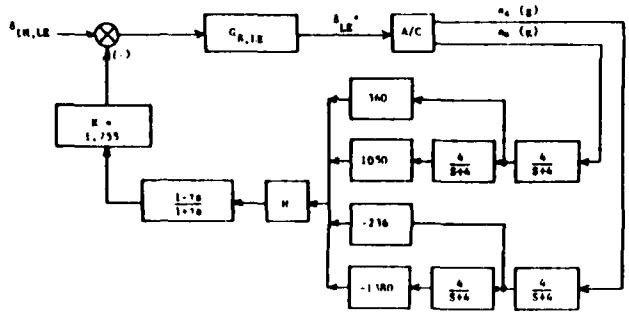

$G_{S,LF}$ has a nominal gain of 0DB

The feedback loops have a unit of n/g

T maximum = 0.027B second

Test Point 16A, B_1 = 1.60, B_2 = 1.05, B_3 = 2.16, B_4 = 1.18, B_5 = 2.25, B_6 = 0

Figure 16. The British Control Law (BAE).

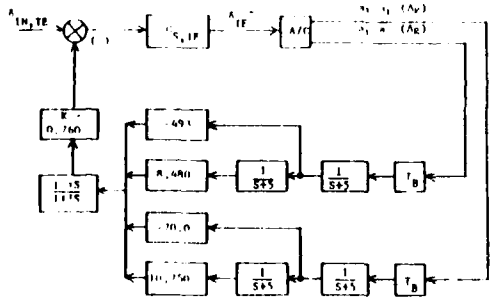

$G_{S,LF}$ has a nominal gain of 0DB.

The feedback loops have a unit of n/dg

Test Point 291, B_1 = 4.91, B_2 = 8.68, B_3 = 7.00, B_4 = 1.075, B_5 = 10.00, B_6 = 0, T = 0

Figure 17. The German Control Law (MBB).

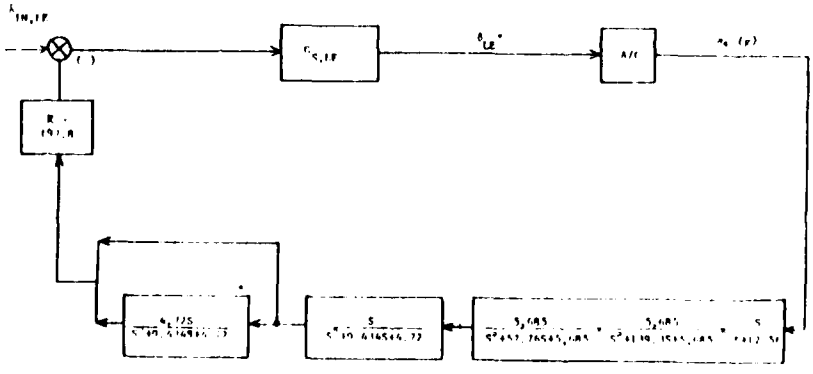

$G_{S,LF}$ has a nominal gain of 0DB.

The feedback loop has a unit of n/g

Test Point 423, B_1 = 5.10, B_2 = 5.00

B_1 controls the overall gain K of the feedback loop

B_2 controls the output level of the block marked by the asterisk *

Figure 18. The French Control Law (ON).

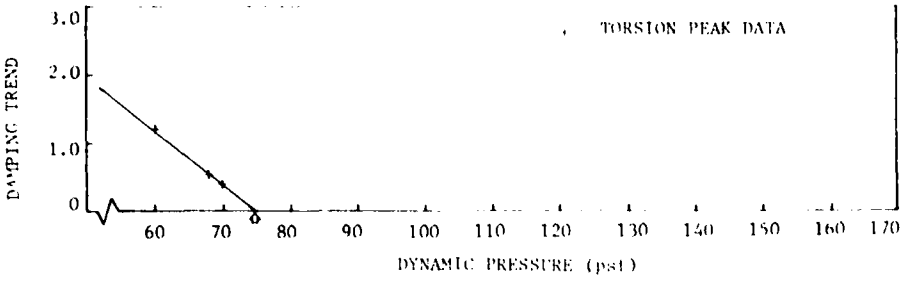

Figure 19. Damping Trend of the YF-17 Flutter Suppression Model - Open Loop M = 0.80.

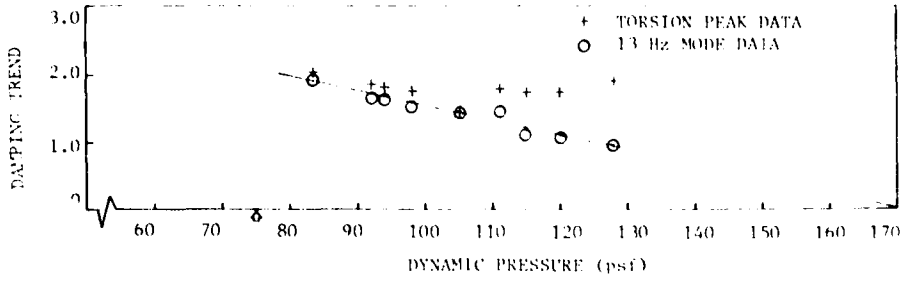

Figure 20. Damping Trend of the Northrop Leading Edge Surface Control Law - N1 (TP89-103).

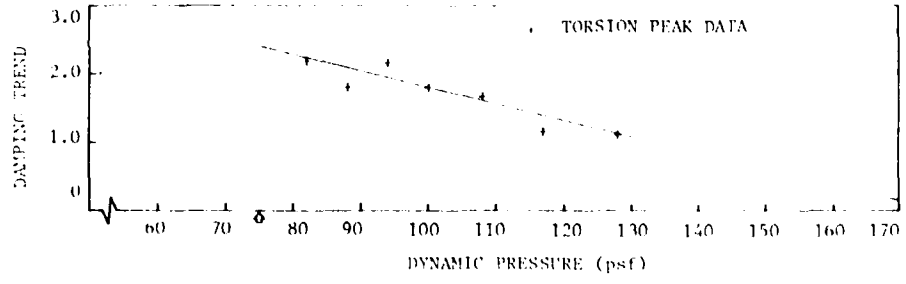

Figure 21. Damping Trend of the Northrop Three Transducer Control Law - N3 (TP 117-127).

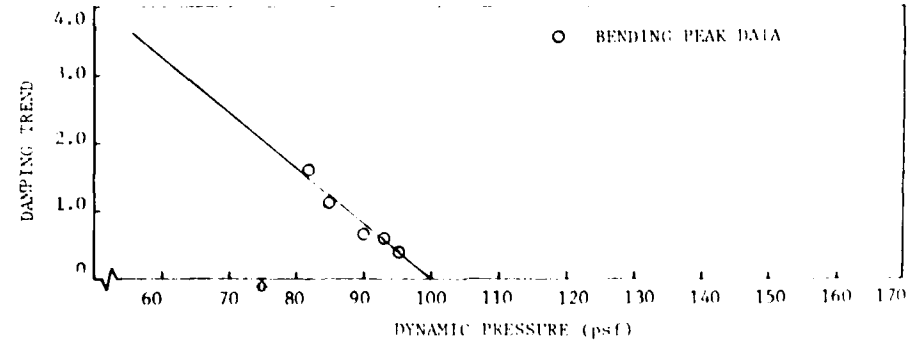

Figure 22. Damping Trend of the Modified Northrop Trailing Edge Surface Control Law - N3T (TP 245-249).

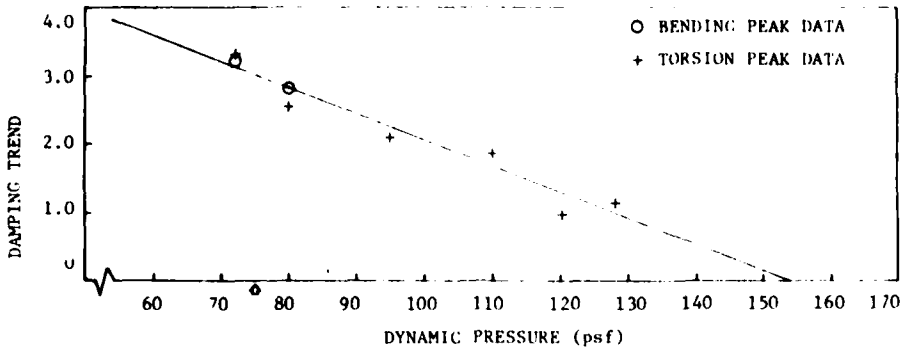

Figure 23. Damping Trend of the Northrop Two Surface Control Law - N3P (TP 487-508).

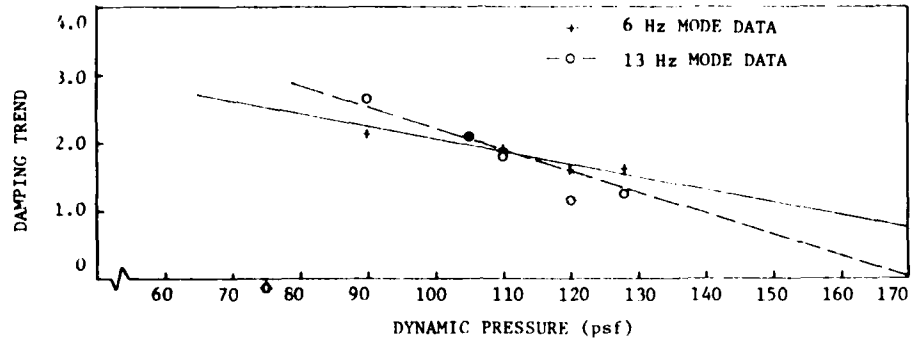

Figure 24. Damping Trend of the British Control Law, BAE (TP 180-212).

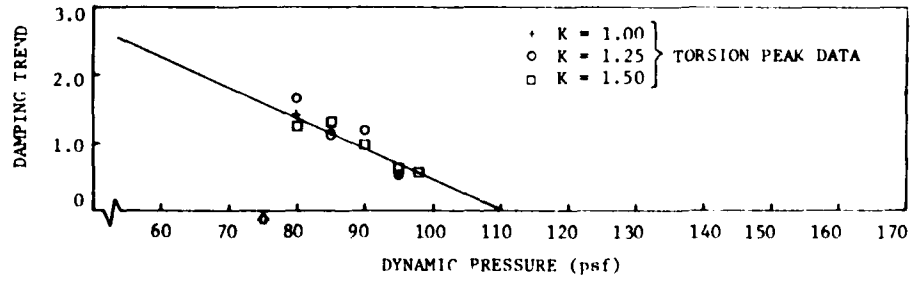

Figure 25. Damping Trend of the German Control Law - MBB (TP 338-356).

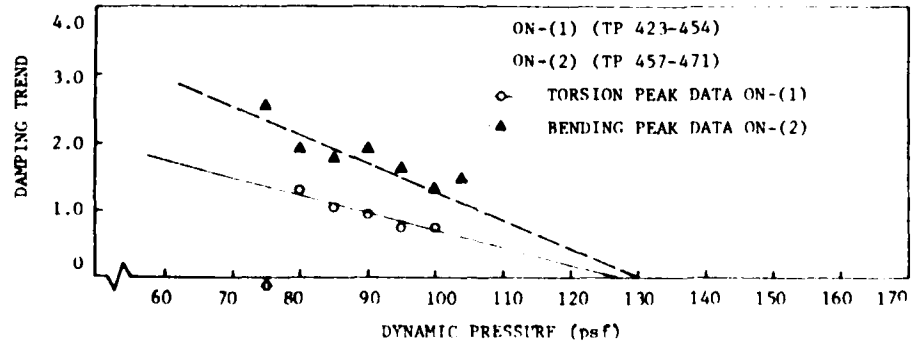

Figure 26. Damping Trend of the French Control Law - ON.

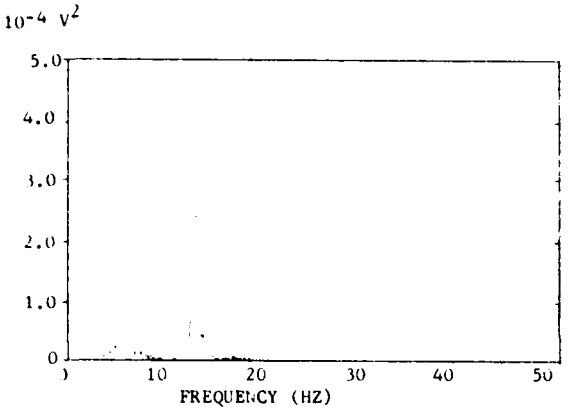

Figure 27. The PSD of the Leading Edge Surface Angular Displacement Acquired at Test Point 104, Q = 128 psf, Control Law N1.

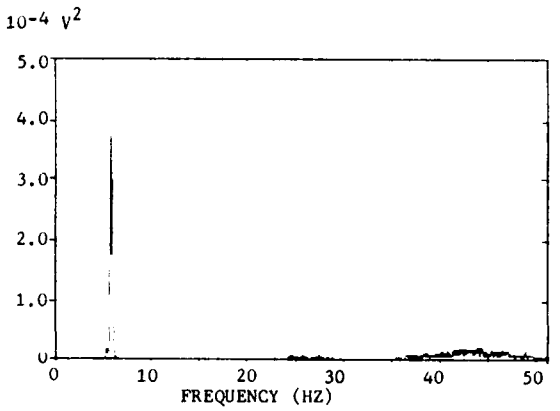

Figure 30. The PSD of the Wing Root Torsion Gage Output Acquired at Test Point 64, Open Loop, Q = 73 psf.

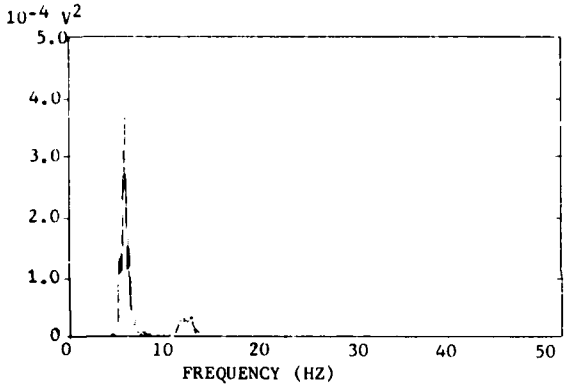

Figure 28. The PSD of the Leading Edge Surface Angular Displacement Acquired at Test Point 127, Q = 128 psf, Control Law N3.

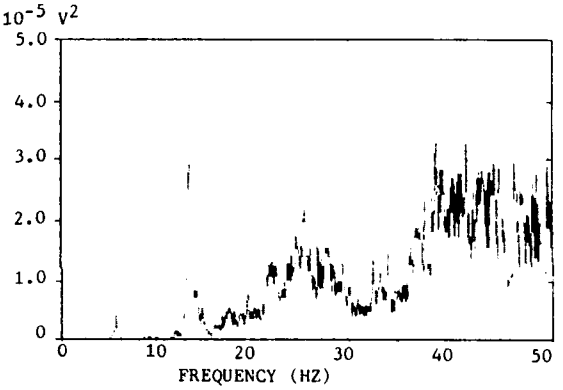

Figure 31. The PSD of the Wing Root Torsion Gage Output Acquired at Test Point 104, Q = 128 psf, Control Law N1.

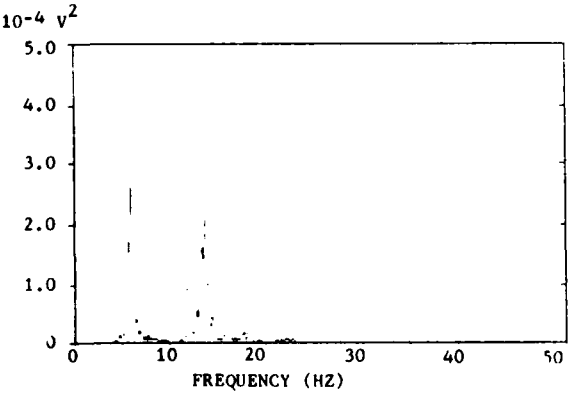

Figure 29. The PSD of the Leading Edge Surface Angular Displacement Acquired at Test Point 211, Q = 128 psf, Control Law BAE, K = 1.20.

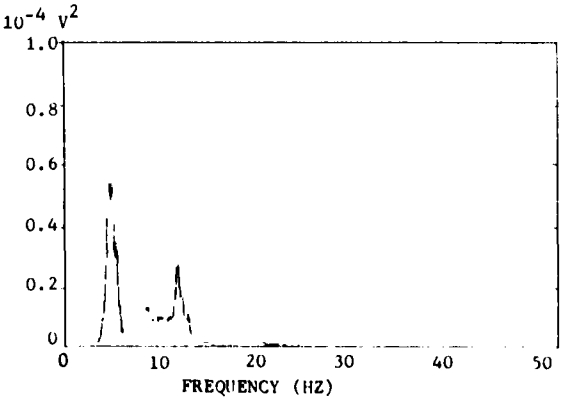

Figure 32. The PSD of the Leading Edge Surface Angular Displacement Acquired at Test Point 510, Q = 128 psf, Control Law N3P.

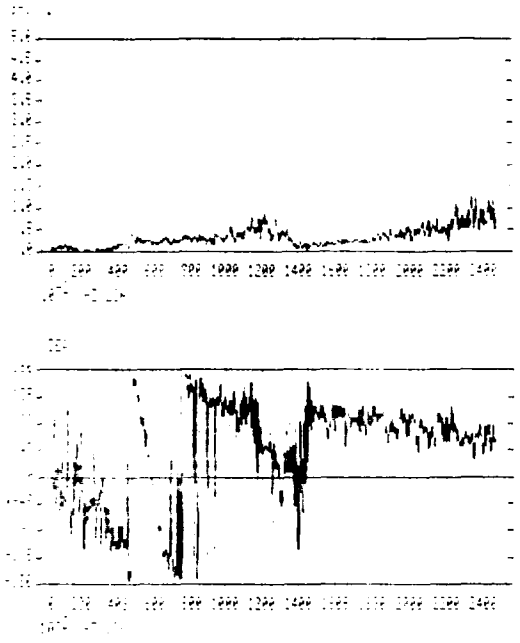

Figure 33. Transfer Function ($a_3 - a_1$) Versus $\delta_{IN,LE}$. Test Point 506, Q = 95 psf. Control Law N3P.

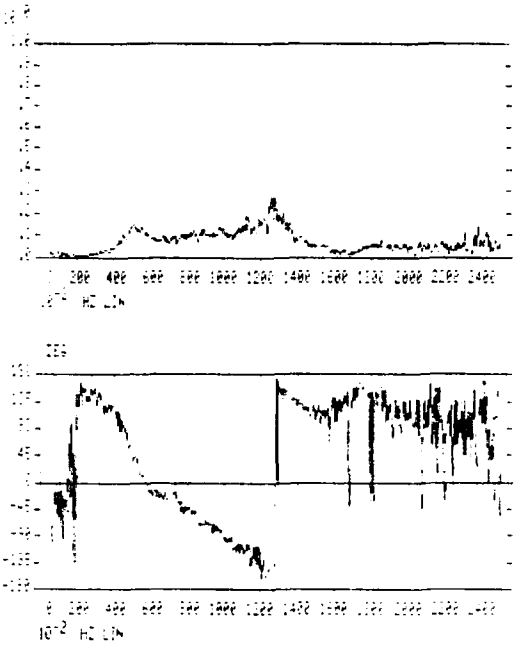

Figure 35. Transfer Function ($a_3 - a_1$) Versus $\delta_{IN,TE}$. Test Point 507, Q = 95 psf. Control Law N3P.

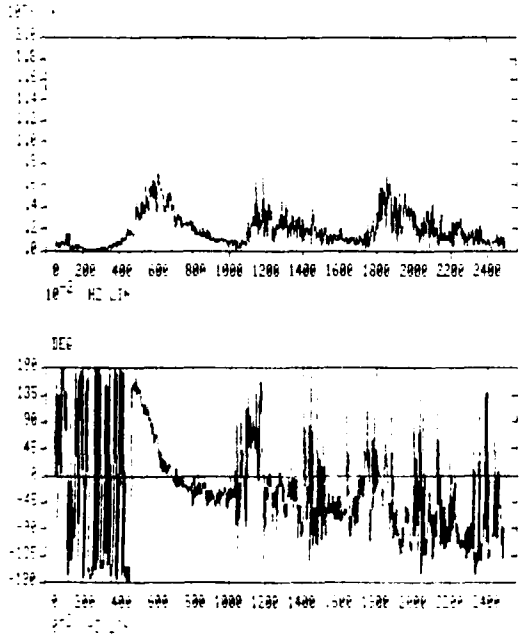

Figure 34. Transfer Function ($a_4 - a_3$) Versus $\delta_{IN,LE}$. Test Point 506, Q = 95 psf. Control Law N3P.

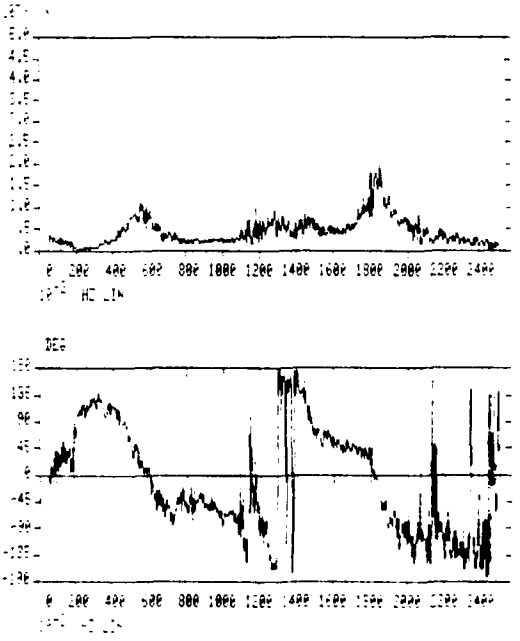

Figure 36. Transfer Function ($a_4 - a_3$) Versus $\delta_{IN,TE}$. Test Point 507, Q = 95 psf. Control Law N3P.

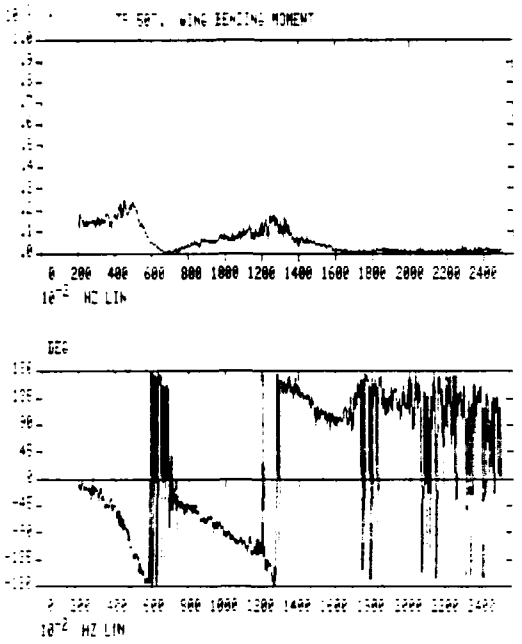

Figure 37. Transfer Function of the Wing Bending Moment Gage Versus $\delta_{IN,TE}$. Test Point 507, Q = 95 psf, Control Law N3P.

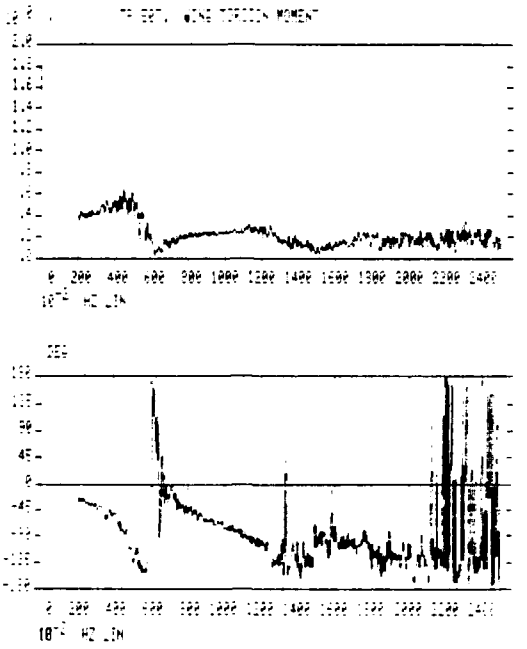

Figure 38. Transfer Function of the Wing Torsional Moment Gage Versus $\delta_{IN,TE}$. Test Point 507, Q = 95 psf, Control Law N3P.

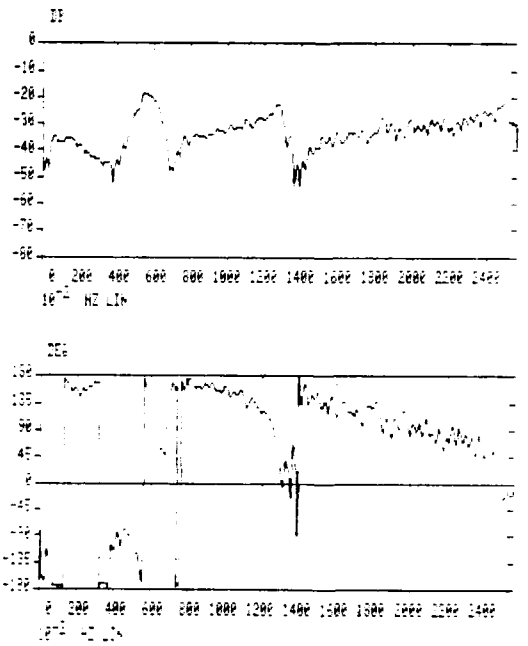

Figure 39. Smoothed Closed Loop Transfer Function $(a_3 - a_1)$ Versus $\delta_{IN,LE}$ Acquired at Test Point 504, M = 0.80, Q = 95 psf, Control Law N3.

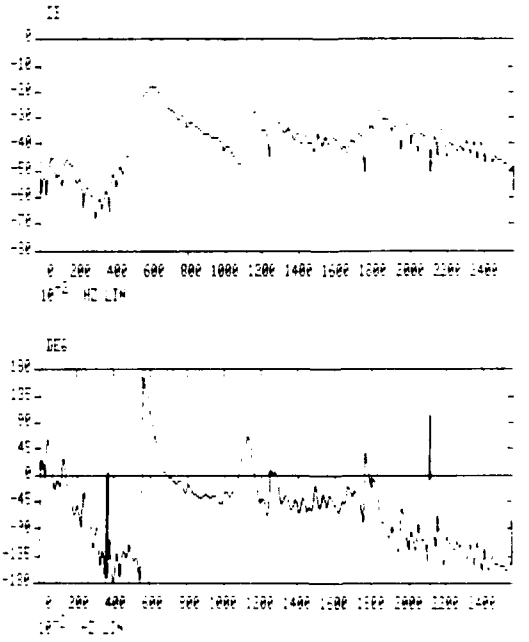

Figure 40. Smoothed Closed Loop Transfer Function $(a_4 - a_3)$ Versus $\delta_{IN,LE}$ Acquired at Test Point 504, M = 0.8, Q = 95 psf, Control Law N3.

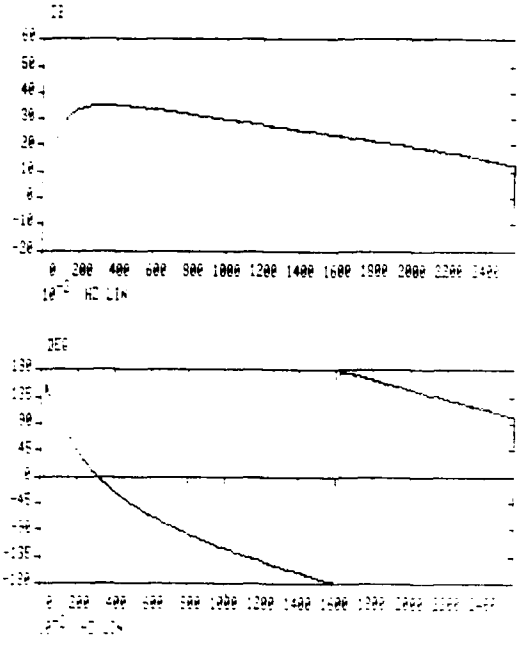

Figure 41a. Compensation Filter F_1H. Refer to Figure 7.

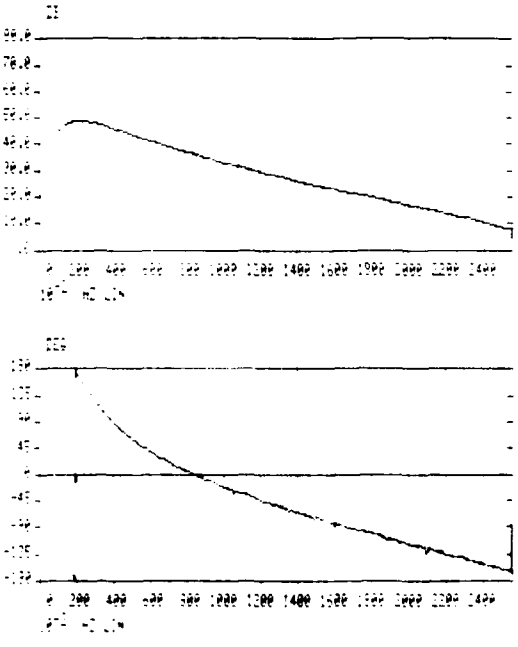

Figure 41b. Compensation Filter F_2H.

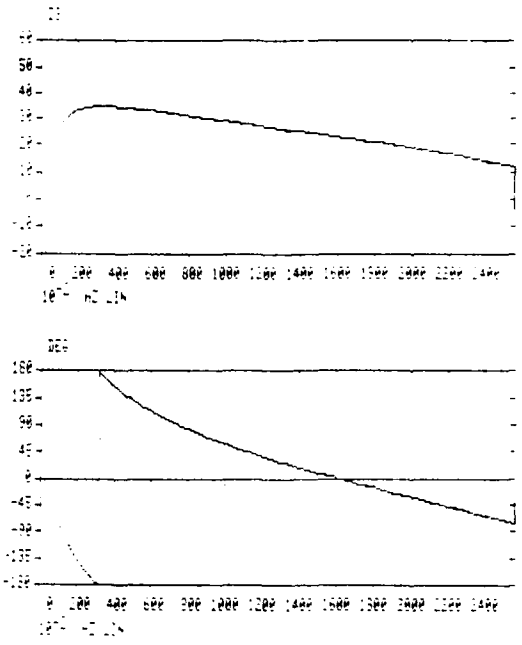

Figure 41c. Compensation Filter F_3H.

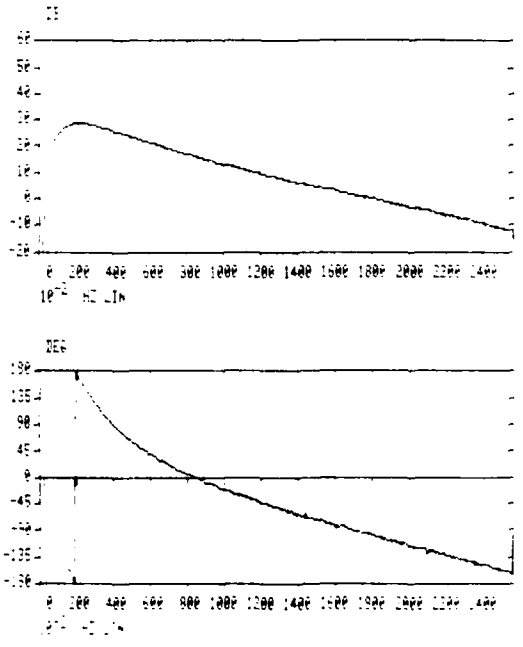

Figure 41d. Compensation Filter F_4H.

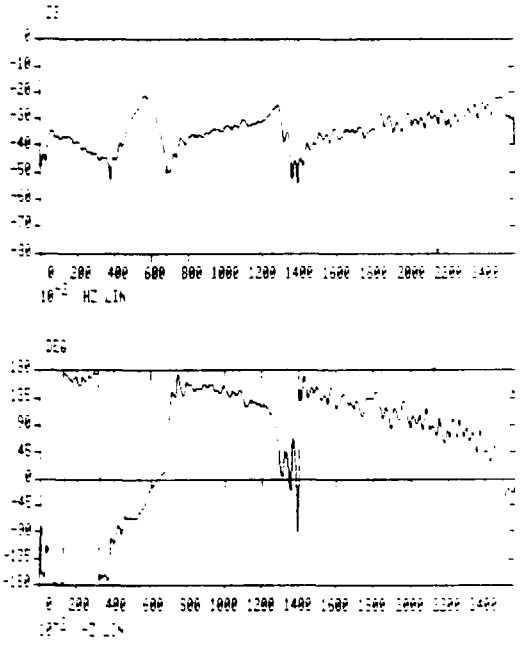

Figure 42. Extracted Open Loop Transfer Function ($a_3 - a_1$) Versus the Leading Edge Control Surface Input $\delta_{IN,LE}$. M = 0.8, Q = 95 psf.

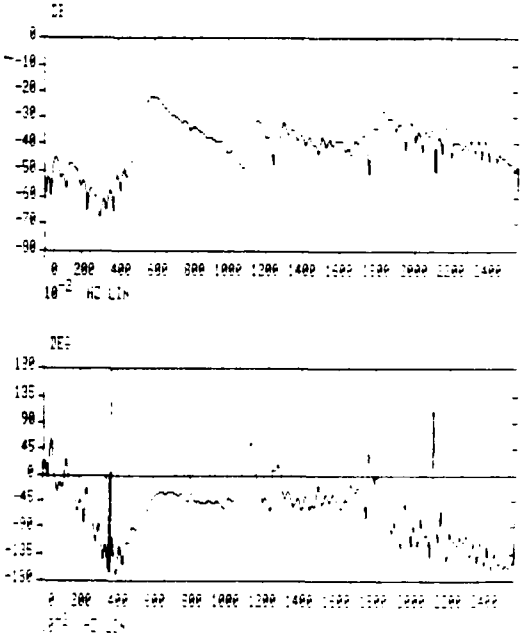

Figure 43. Extracted Open Transfer Function ($a_4 - a_3$) Versus the Leading Edge Control Surface Input $\delta_{IN,LE}$. M = 0.8, Q = 95 psf.

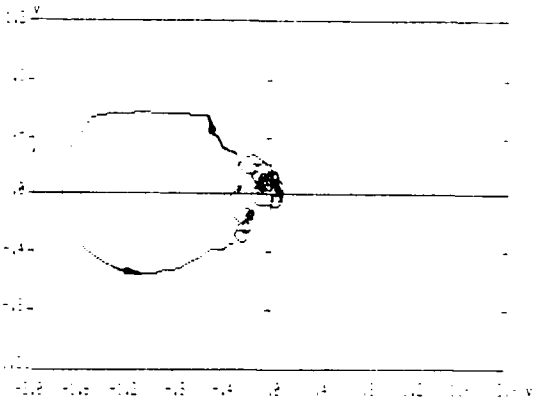

Figure 44. Open Loop Nyquist Plot for the Example Presented in Figures 39 Through 43. The Test Condition was M = 0.8, Q = 95 psf, which is 27% Above the Critical Open Loop Flutter Dynamic Pressure.

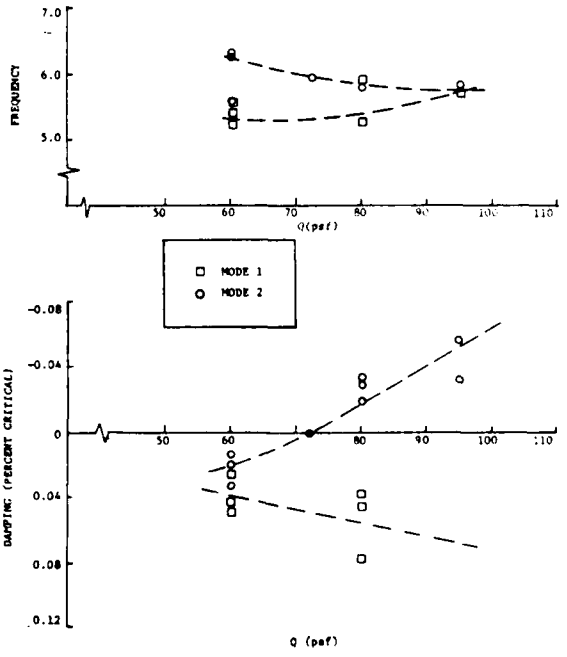

Figure 45. Open Loop Flutter Results from the Wind Tunnel Test.

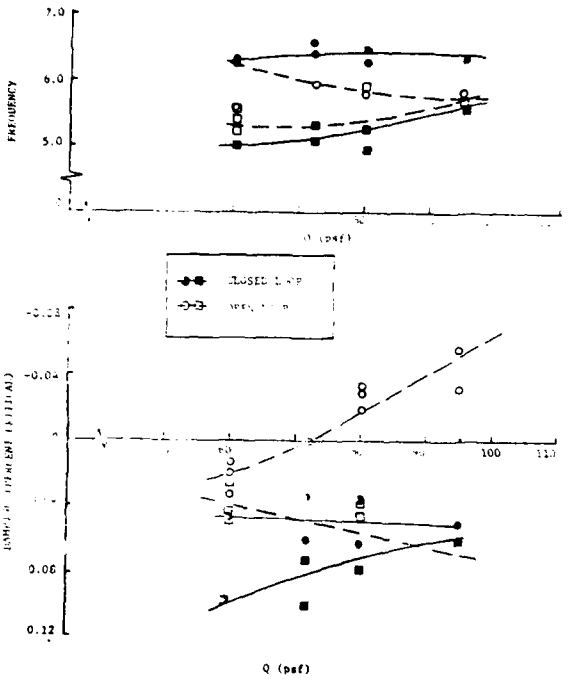

Figure 46. Northrop Control Law (N3) Wind Tunnel Results.

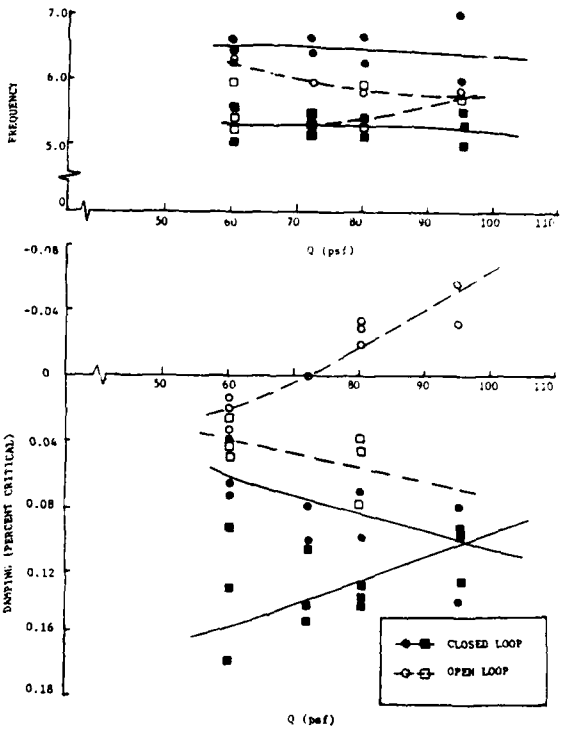

Figure 48. Northrop Leading and Trailing Edge Control Law (N3P) Wind Tunnel Results.

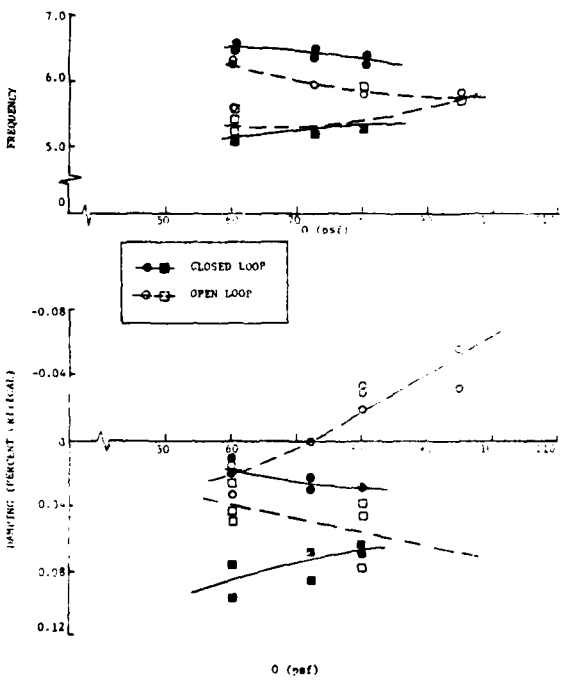

Figure 47. Northrop Trailing Edge Law (N3T) Wind Tunnel Results.

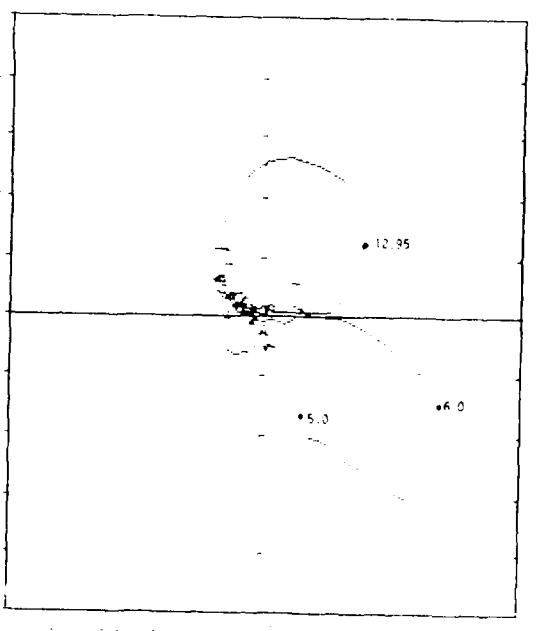

Figure 49. Experimental Open Loop Polar Plot of Transfer Function $(a_3 - a_1)$ Versus $\delta_{IN,LE}$ at $Q/Q_f = 1.27$.

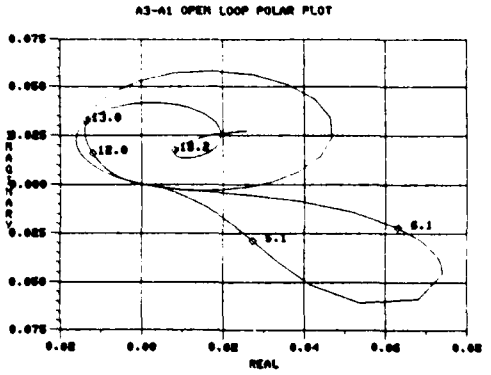

Figure 50. Analytical Open Loop Polar Plot of Transfer Function ($a_3 - a_1$) Versus $\delta_{IN,LE}$ at $Q/Q_f = 1.27$.

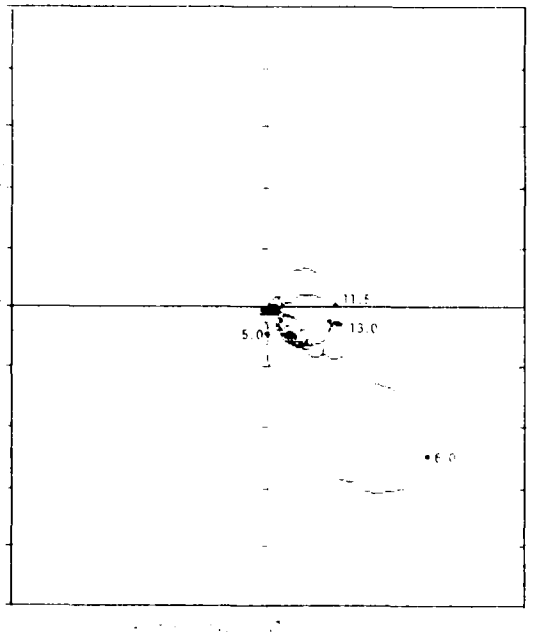

Figure 51. Experimental Open Loop Polar Plot of Transfer Function ($a_4 - a_3$) Versus δ_{LE} at $Q/Q_f = 1.27$.

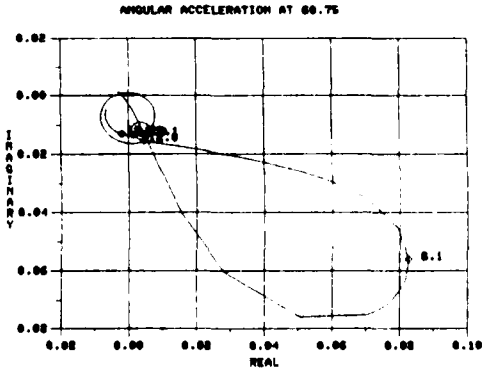

Figure 52. Analytical Open Loop Polar Plot of Transfer Function ($a_4 - a_3$) Versus $\delta_{IN,LE}$ at $Q/Q_f = 1.30$.

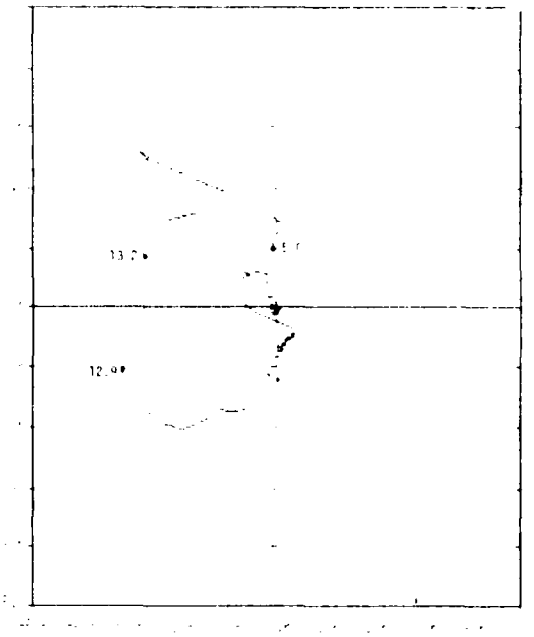

Figure 53. Experimental Open Loop Polar Plot of Transfer Function ($a_3 - a_1$) Versus $\delta_{IN,TE}$ at $Q/Q_f = 1.07$.

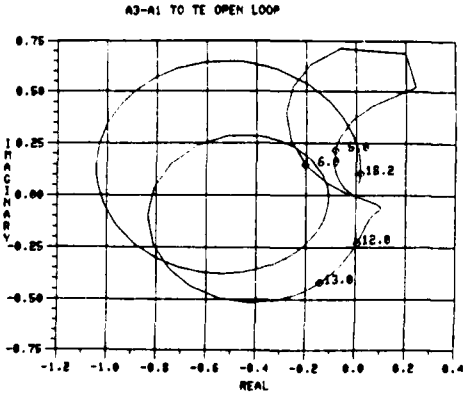

Figure 54. Analytical Open Loop Polar Plot of Transfer Function ($a_3 - a_1$) Versus $\delta_{IN,TE}$ at $Q/Q_f = 1.07$.

ACTIVE CONTROL OF AN EXPLOSIVE WING-STORE FLUTTER CASE

by

H.Hönlinger
O.Sensburg
M.Kühn
H.Gödel

MESSERSCHMITT-BÖLKOW-BLOHM GmbH.
Airplane Division
P.O. Box 80 11 60, 8000 Munich 80
W.-Germany

SUMMARY

Control laws were calculated, using optimal control theory, to suppress an explosive wing-store flutter case on a YF-17 dynamically scaled model. The trailing edge flap was used for flutter suppression because usually hydraulically driven ailerons are available in modern fighters. The design aim of 1.5 times the flutter dynamic pressure could be demonstrated during the wind tunnel test. It should be emphasized that no changes to the analytically developped control law were neccessary in the test which proves that theory has well advanced during the last years.

INTRODUCTION

In addition to the joint F4 flutter suppression program of the U.S. Air Force Flight Dynamics Laboratory and the MBB-Airplane Division Control Laws were calculated by MBB for active control of an explosive wing store flutter case. These control laws were implemented into a dynamically scaled model of the YF-17 aircraft by the Northrop Corporation Aircraft Group and tested in the 16 ft Freon Wind Tunnel of the NASA Langley Research Center. Design aim was to reach 1.5 the flutter dynamic pressure with the control system on. This goal could be fulfilled but the necessary safety margins could not be met. An improved system was laid out afterwards analytically which would meet the required margins. Since good correlation of test results with the first set of control laws was found it is believed that the improved system would also behave as predicted in the wind tunnel. The work performed by MBB during this program was sponsored by the ZTL-Research Program of the German Ministry of Defense. The wind tunnel program was procured by the AFFDL.

A complete description of the whole program which involved the cooperation of several countries is given in /1/.

1. SYSTEM DESCRIPTION

The flutter model used is a 30% scale half model of the YF-17 with an empty tip launcher rail and an AIM-75 missile attached to a pylon. A picture of the model is presented in Fig. 1. The model was equipped with a hydraulically driven leading edge and trailing edge flap and three accelerometers which provided the feedback signals for our control laws. The actuator transfer function is shown in Fig. 2 . A ground resonance test was performed on the model with the tunnel support conditions simulated /2/. Fig. 3 presents the measured mode shapes of Mode I to Mode IV. The flutter calculation in Fig. 4 shows classical wing bending (Mode I) - wing torsion (Mode II) flutter. It can also be seen in this figure that the system reduced to a binary system behaves almost identical which is very useful for applying optimal control theory with complete state vector feedback. All control laws were laid out considering Mode I and Mode II only.

2. ANALYTICAL APPROACH

Unsteady Aerodynamic Forces

Unsteady aerodynamic forces were performed using eight measured vibration modes of the model. The rigid body modes were neglected. For the unsteady aerodynamic forces the following simplifications were made.

- It was assumed that the aerodynamic forces of the tailplane have no influence on the wing flutter mechanism. Therefore only the wing aerodynamic unsteady forces were introduced into the calculation.
- The lift of the missile body and the missile-wing interference were neglected.

The unsteady wing aerodynamic forces were calculated for the eight measured e
of the model by the doublet lattice method /3/ and by the lifting surface method

The flutter calculation was performed at Ma = 0.8. Results for the eight degrees o
freedom system are given in Fig. 4.

Because theory overpredicts control surface unsteady airforces the trailing edge lift coefficient was multiplied with a factor of 0.7. There are several unsteady pressure distribution measurements in the transonic regime which prove this correction /5/, /6/.

Control Law Definition

The technical approach to find the control law is described in /7/.

To get the optimal control law k_{opt} the quadratic performance criterion is minimized

$$J = \int_0^{\infty} (\{x\}^T [Q] \{x\} + x_i R x_i) \, dt$$

Q is a weighting matrix found by trial and error by using a screen together with the computer. R is a scalar, to be selected, because there is only one control surface. X is the state vector and Xi is the actuator input signal.

Minimizing (J) leads to the optimal control laws

$$x_i = \{k_{opt}\}^T \{x\}$$

with

$$\{k_{opt}\}^T = R^{-1} \{B\}^T [P]$$

where P is the steady state solution of the Matrix Riccati equation

$$[P] \cdot [P][A] + [A]^T [P] - [P][B] R^{-1} [B]^T [P] + [Q]$$

Because there is no direct access to the state vector x, linear combinations of the sensor outputs can be used to get the state terms

$$\{y\} = [C] \{x\}$$

where y is the sensor output and C a transformation matrix.

The following sketch shows the block diagram for this model.

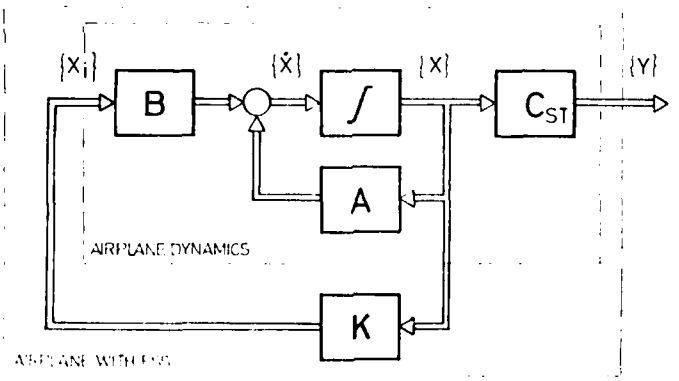

The control vector K_m related to the measured vector y can be defined by the inverse transformation matrix C-1

$$\{K_m\}^T = \{K_{opt}\}^T [C^{-1}]$$

No problem arises to perform equation above if the complete state vector is fed back thus leading to a quadratic form of the transformation matrix C.

The flutter case can be described by two modes

- first wing bending q_1
- first wing torsion + store pitch q_2

These modes can be measured by three accelerometers on the wing. For the realization of the control law it was found that contribution of the states related to the aileron is small and therefore no feed back of those states is necessary.

The block diagram of the control law realized for tunnel testing is shown in Fig. 5. The factors kϑ, Kϑ̇ are related to the wing torsion and Kφ , Kφ̇ are related to the wing bending. It was also possible to change the total gain and the total phase of the actuator input signal X_i.

The control law was found by using only two generalized coordinates (wing bending - wing torsion) as feedback. When the total vibration system is used then there is always the possibility that adverse signals are picked up because the measured vector contains contributions from all modes. A flutter calculation plot is presented in Fig. 6 which shows that Mode IV (fuselage first bending, Fig. 3) becomes unstable. There is considerable motion of the outer wing on this mode. The Nyquist plot of Fig. 7 shows a perfect circle for the torsion mode with sufficient gain and phase margin (6 db ± 60°). It also shows a mode at about 12.8 Hz (Mode IV) to be unstable because the point -1 is encircled from the left side. The bandpass filter of Fig. 8 was incorporated. The effect of this filter was compensated only at 6 Hz by shifting the control law forward about 80° (which means just other factors for $K\phi$, $K\dot{\phi}$, K_Θ, $K\dot{\Theta}$ of Fig. 5).

A Nyquist plot for this new control law is presented in Fig. 9 which shows Mode IV to be stable but the circle at 6 Hz is deteriorated (there is less phase margin now!). An adverse behaviour of this control law is also shown in the v-g plot of Fig. 10. The flutter speed is reduced about 10 kts (compared to Fig. 6) and the damping behaviour is much more explosive because now the bending mode is fluttering.

3. WIND TUNNEL TEST RESULTS

The peak hold spectrum method was extensively used to find the model flutter speeds with and without flutter control. The method provides power spectrum density values for different signals. The input signal is wind tunnel noise.

Typical examples of this method are plotted in Fig. 11. The inverse of the amplitude for the two peaks of Fig. 11 is plotted in Fig. 12 versus speed. The model flutters at the speed where this value is zero. Fig. 11 indicates the same behaviour as shown in the v-g plot of Fig. 10. Whereas the torsional mode is suppressed with increasing speed the bending mode becomes unstable. Fig. 13 shows the model flutter speed versus total gain of the flutter suppression system. From this figure it can be deduced that an increase in gain above 0.7 increases the flutter speed very little and would only make the systems very sensitive to disturbances. The phase margins of ± 60° could not be fulfilled with this control law whereas the 6 db gain margin can almost be met.

Fig. 14 shows good correlation of test results with analytical predictions.

4. IMPROVED FLUTTER SUPPRESSION SYSTEM

After consideration of wind tunnel test results and a review of control law finding procedures, two major deficiencies were found

- the band pass filter used had large phase shifts in the range from 4 Hz to 8 Hz (about 90° phase lag)
- it was not included in the optimization procedure but just compensated for one distinct frequency.

A band pass filter was designed which had almost the same attenuation behaviour as the one used in the test, but had much less phase shift in the range 4 Hz to 8 Hz (about 20° phase lag). The filter behaviour is shown in Fig. 15.

The filter transfer function was multiplied with the actuator transfer function and approximated at the design frequency. So the filter function was already included when optimal control theory in the time domain was applied and new control laws were found.

Analytical Results for the improved System

Having found the new control vector, a Nyquist diagram was made at the design speed of 280 kts. This diagram (Fig. 16) shows now a perfect circle. The v-g plot of Fig. 17 also shows a much less critical damping behaviour (compared to Fig. 10). It is always the torsion mode which becomes unstable.

Figures 18, 19, 20 show the results of sensitivity studies were the system total gain and the phase shift of the actuator input signal were investigated. Again it is proven that the best control law is the one produced by applying optimal control theory ($K = 1.0$, $\varphi = 0$).

Fig. 18 shows a stable system with a flutter speed of 350 kts for $K = 1.5$. With a 6 db gain margin 300 kts flutter speed could be achieved which is above our design goal. The phase margins are still below the desired ± 60° phase shifts as is presented in Fig. 19 and Fig. 20. For an operational system one would have to control the phase of the total system very closely - possibly by means of self measuring and self adjusting.

REFERENCES

/1/ HWANG, C.
JOHNSON, E.H.
MILLS, G.R.
NOLL, T.E.
FARMER, M.G.

Wind Tunnel Test of a Fighter Aircraft Wing/ Store Flutter Suppression System - An International Effort

Paper presented on the 50th Meeting of the SMP of AGARD, 13-18 April 1980, Athens/Greece

/2/ VOELKER, L.S.

Ground Vibration Test of the Active Flutter Suppression Transonic Model with External Stores

AFFDL-TM-77-92-FBR

/3/ GIESING, J.G.
KALMAN, T.P.
RODDEN, W.P.

Subsonic Unsteady Aerodynamics for General Configurations

AIAA-Paper 72-76, 1972

/4/ LASCHKA, B.

Zur Theorie der harmonisch schwingenden tragenden Fläche bei Unterschallströmung

ZfW, Heft 7, 1963

/5/ DESTUYNDER, R.
HÖNLINGER, H.

Active Control Technology for Flutter Suppression

VKI-Lecture Series, 4-8 Dec. 1978, Brussels/Belgium

/6/ LODGE, C.G.
SCHMID, H.

Unsteady Pressures due to Control Surface Rotation at low Supersonic Speeds, Comparison between Theory and Experiment

AGARD Report No. 647 (1976)

/7/ SENSBURG, O.
HÖNLINGER, H.
NOLL, T.E.

Active Flutter Suppression on a F-4F Aircraft with External Stores using Already Existing Control Surfaces

Paper presented on the 21st Structures, Structural Dynamics and Materials Conference of the AIAA, 12-14 May 1980, Seattle/Washington, U.S.A.

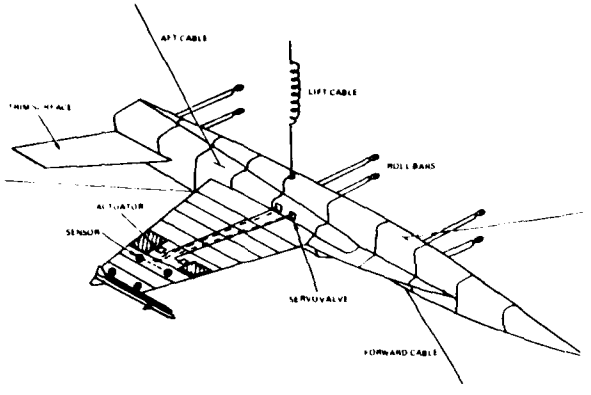

FIG. 1 YF-17 MODEL AND MODEL SUSPENSION

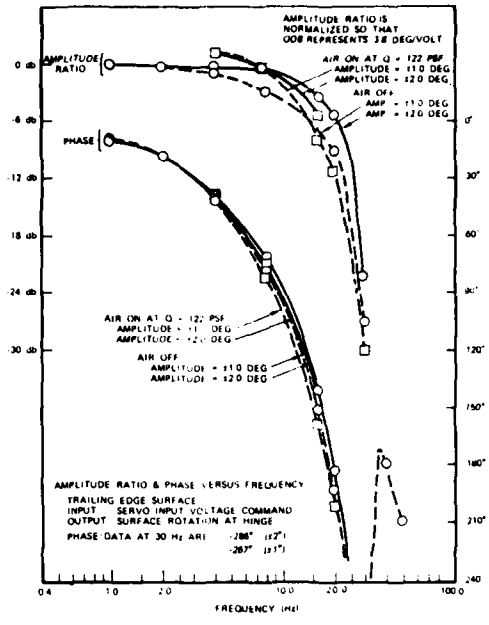

FIG. 2 TRAILING EDGE FLAP ACTUATOR TRANSFER FUNCTION

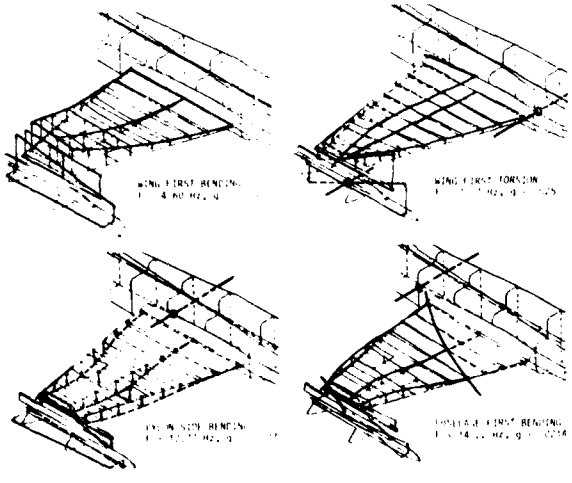

FIG. 3 MEASURED MODE SHAPES OF THE MODEL

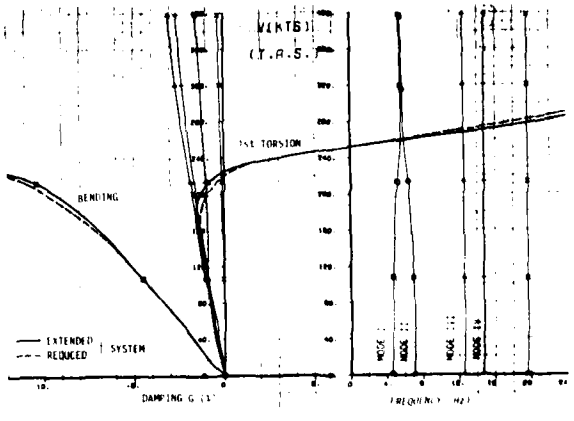

FIG. 4 FLUTTER CALCULATION WITH EXTENDED AND REDUCED SYSTEM

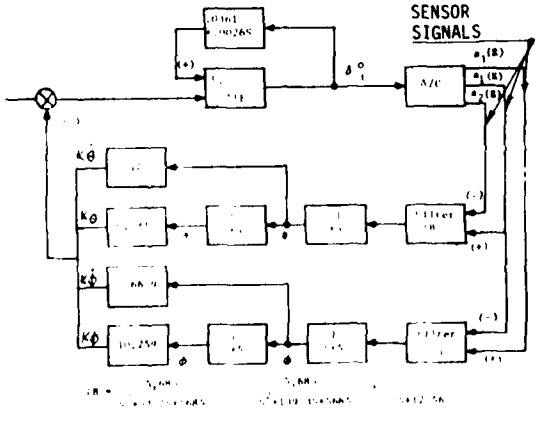

FIG. 5 BLOCK DIAGRAM OF THE CONTROL LAW TESTED IN THE WIND TUNNEL

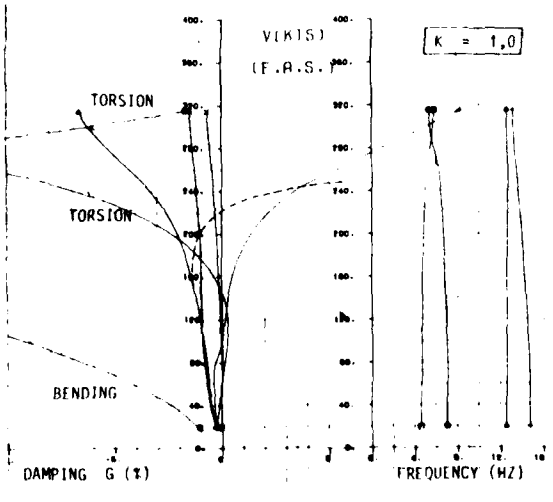

FIG. 6 V-G PLOT OF CONTROL LAW WITHOUT BANDPASS

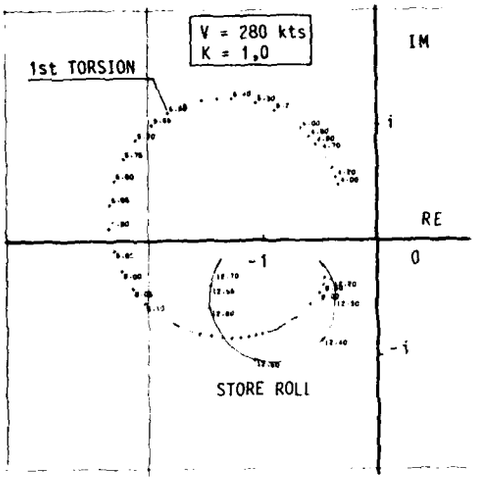

FIG. 7 NYQUIST DIAGRAM WITHOUT BANDPASS

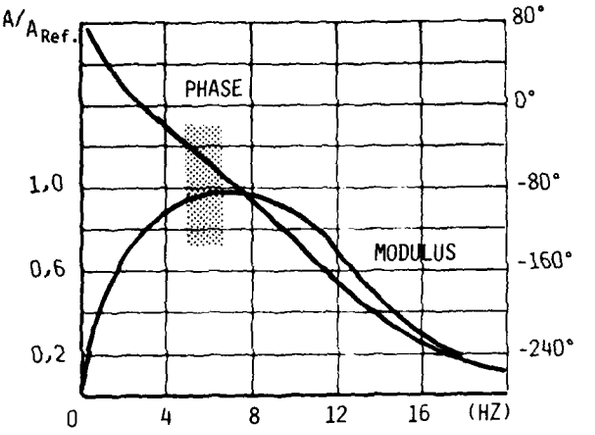

FIG. 8 ONERA BANDPASS FILTER

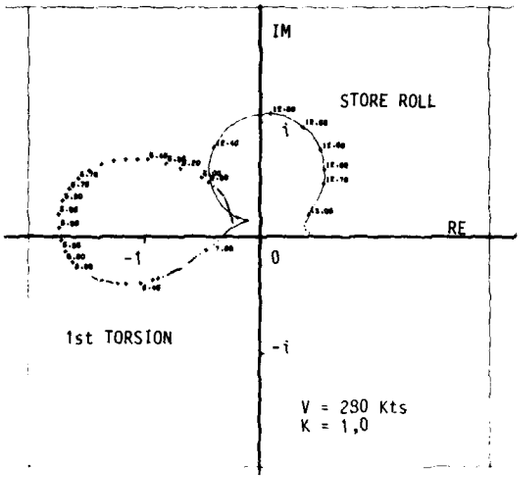

FIG. 9 NYQUIST DIAGRAM OF CONTROL LAW WITH ONERA BANDPASS FILTER

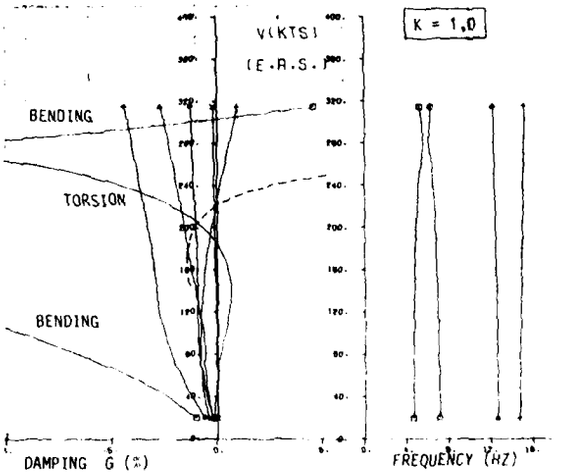

FIG. 10 V-G PLOT OF CONTROL LAW WITH ONERA BANDPASS FILTER

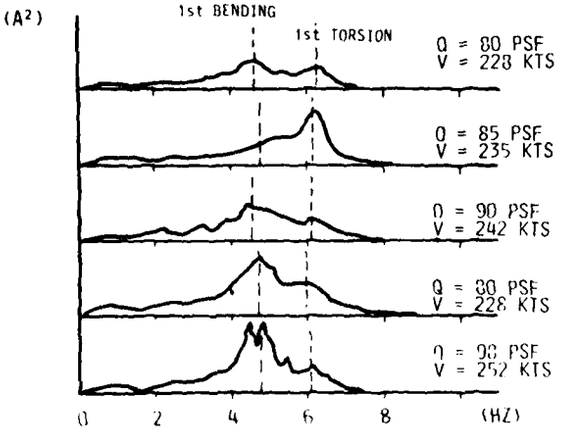

FIG. 11 PEAK HOLD DIAGRAMS FOR VARIOUS SPEEDS AT M = 0,8; K = 1,0

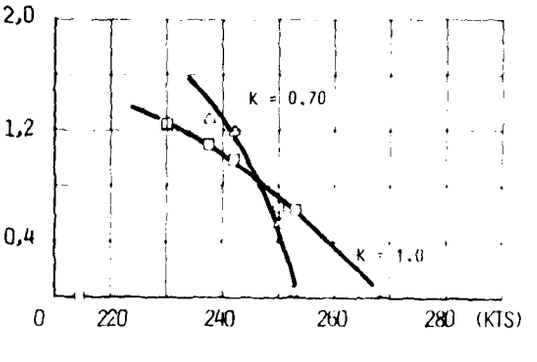

FIG. 12 INVERSE AMPLITUDE VS SPEED

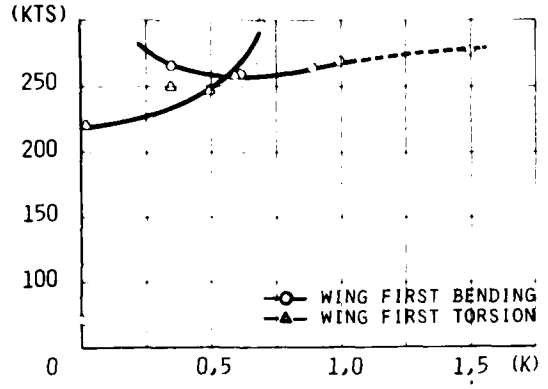

FIG. 13 FLUTTER SPEED VS GAIN

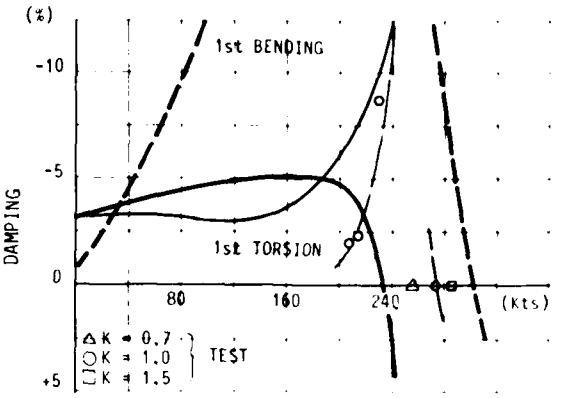

FIG. 14 COMPARISON OF TEST RESULTS AND PREDICTIONS

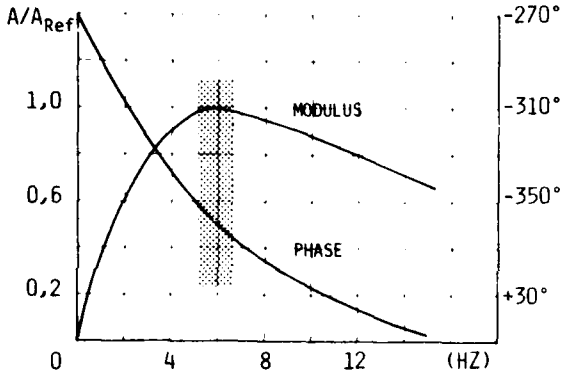

FIG. 15 MBB BANDPASS FILTER

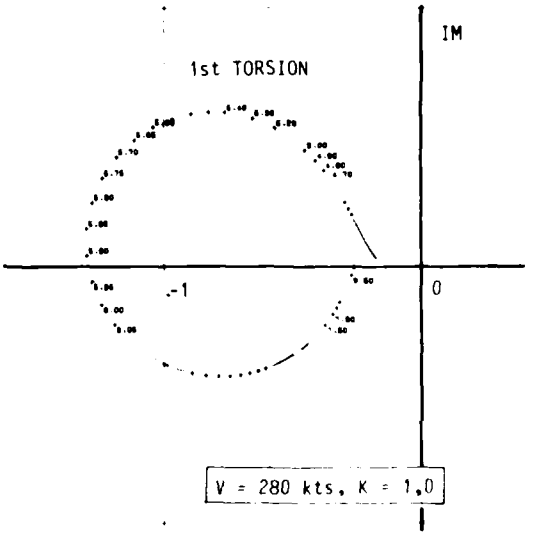

FIG. 16 NYQUIST DIAGRAM OF IMPROVED CONTROL LAW WITH MBB BANDPASS FILTER

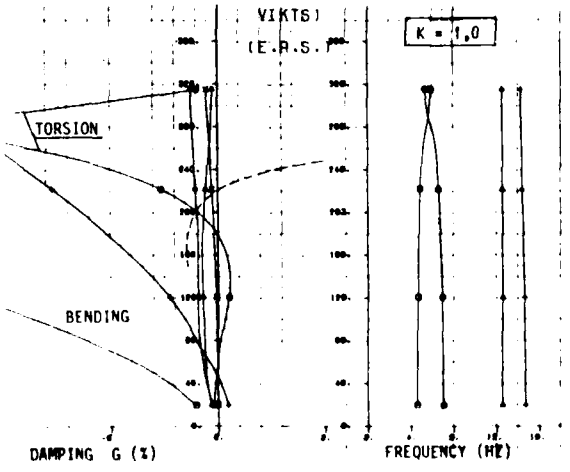

FIG. 17 V-G PLOT OF IMPROVED CONTROL LAW WITH MBB FILTER

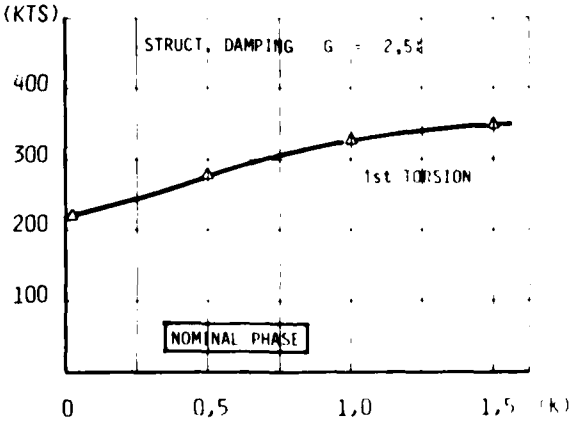

FIG. 18 FLUTTER SPEED VS GAIN

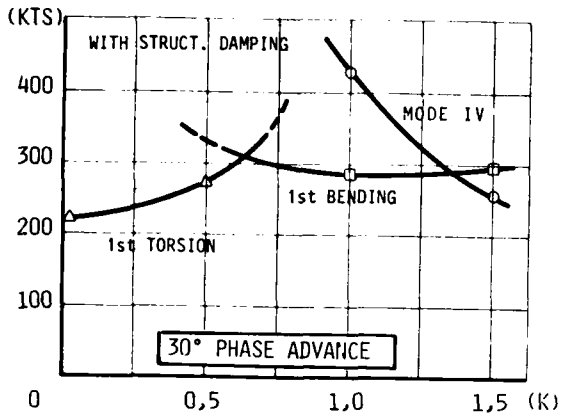

FIG. 19 FLUTTER SPEEDS VS GAIN

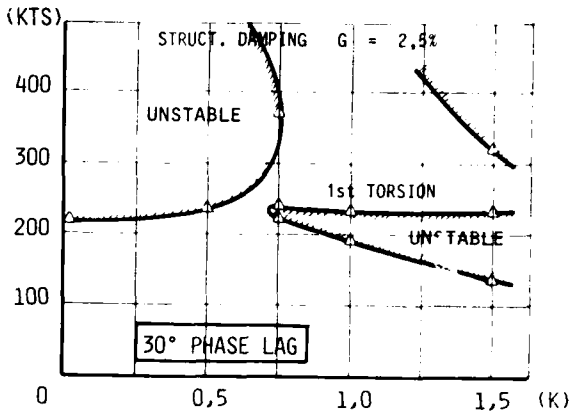

FIG. 20 FLUTTER SPEEDS VS GAIN

ESSAIS EN SOUFFLERIE SUR UNE MAQUETTE DE L'AVION YF17 CONCERNANT LE FLOTTEMENT D'UNE COMBINAISON AILE-ENGIN (COOPERATION INTERNATIONALE)

Par Roger DESTUYNDER

Office National d'Etudes et de Recherches Aérospatiales (ONERA)
29, Avenue de la Division Leclerc
92320 CHATILLON - France

RESUME

Une optimisation d'une loi de contrôle de flottement a été recherchée pour le cas de la maquette de l'avion YF17 équipé d'une charge en bout d'aile (configuration B).

La loi de contrôle appliquée est basée sur le principe de la réinjection d'une rigidité sur l'aile par l'intermédiaire des forces aérodynamiques instationnaires induites par rotation d'une gouverne.

Dans le cas présent on a utilisé pour le contrôle la gouverne de bord d'attaque et un seul accéléromètre placé sur l'aile près de la ligne de noeud du mode de tangage de la charge. Lors du passage en soufflerie on a strictement utilisé la loi de contrôle nominale sans chercher à tenir compte des différences qui pouvaient exister entre les modes et les fréquences utilisés dans le calcul avec les modes et les fréquences réels lors du passage en soufflerie.

Le contrôle à Mach 0,80 a permis d'augmenter de façon importante la pression dynamique critique et surtout de réduire considérablement l'explosivité du phénomène de flottement. La comparaison entre les prévisions de calcul et les essais est satisfaisante aussi bien du point de vue qualitatif que quantitatif.

TEST AND ANALYSES OF A ACTIVE FLUTTER SUPPRESSION SYSTEM ON A FFDL MODEL OF YF17

SUMMARY

A flutter control law was calculated for a YF17 model equiped with a store at the wing tip.

The control law used stiffness injection on the wing by the help of the unsteady aerodynamic forces induced by a control surface.

In the present case just the leading edge control surface and only one accelerometer mounted on the wing close to the nodal line of the pitching mode of the external store, were used.

During the wind tunnel tests the nominal control law was used without considering the existing differences between eigen modes and frequencies introduced in the calculations and their modes and frequencies existing on the model itself when mounted in the wind tunnel.

The control at constant Mach number M = 0,80, permitted to increase substantially the critical pressure and also to reduce considerably the explosivity of the flutter phenomena.

Comparison between theory and tests is correct qualitatively and quantitatively.

INTRODUCTION

Dans le cadre d'un travail de coopération entre U.S. Air Force et 3 pays européens (Grande-Bretagne, Allemagne Fédérale et France) il a été décidé que chaque pays expérimenterait une loi de contrôle de flottement calculée par lui-même et appliquée à une maquette dynamiquement semblable de l'avion F17. Une charge en bout d'aile était lestée de façon fictive et permettait d'obtenir un flottement très violent à Mach 0,80 dans la soufflerie 16 pieds au fréon de la NASA à Langley Field.

La maquette et les essais étaient sous la responsabilité de la firme Northrop (Fig. 1).

Du côté français l'étude s'est déroulée en trois phases :

a) Montrer que l'on était capable de prévoir correctement le comportement aérodynamique de la maquette jusqu'au flottement sans contrôle.

b) Déterminer une loi de contrôle jugée valable pour ce type de flottement et la comparer avec les résultats expérimentaux.

c) Calculer une loi optimisée à partir des données aérodynamiques déterminées en a) et b).

a) Calcul de flottement

Les calculs de flottement ont été effectués à Mach 0,80, qui était le Mach choisi pour les essais.

Les hypothèses suivantes ont été introduites :

. Les six premiers modes de la maquette ont été considérés (2 modes "rigides" de suspension, translation et tangage et 4 modes de déformation). La gamme de fréquence étudiée s'étendait de 0 à 15 Hz.

. Les forces aérodynamiques instationnaires ont été calculées par une méthode de doublets subsoniques, les surfaces considérées étant l'aile et l'empennage horizontal. Aucune force n'a été introduite sur le pylone ou l'engin AIM75, de la même façon les termes d'interaction volume/empennage et engin-mât/voilure ont été négligés.

. Le couplage est principalement dû aux modes de flexion voilure et tangage engin qui induit une torsion sur l'aile.

. La figure 2 donne l'évolution des paramètres de fréquence et d'amortissement des différents modes en fonction de la densité du fluide dans la soufflerie au fréon à Mach 0,80. Il faut noter la très forte explosivité du phénomène, c'est-à-dire la pente $\frac{\partial \alpha}{\partial \rho}$ du mode critique (ici le mode de tangage).

. Les essais comparatifs qui sont portés sur la figure 3 montrent que, malgré quelques différences dans les données entre calculs et essais, l'allure du phénomène et les ordres de grandeur sont bien prévus.

. Les amortissements et fréquences ont été déterminés expérimentalement à partir de l'enregistrement des couches de densité spectrale moyennées durant 30 secondes en travaillant avec des spectres redondants des réponses à la turbulence naturelle de la soufflerie.

. Différents capteurs privilégiant soit le mode de flexion, soit le mode de tangage de l'engin, ont été utilisés pour suivre l'évolution de ces paramètres.

Cette première partie montrait qu'en ce qui concerne les forces aérodynamiques instationnaires sur l'aile, les hypothèses faites étaient valables, tout au moins au nombre de Mach M = 0,80.

b.1) Calcul de la loi de contrôle

Les équations du flottement s'écrivent en notation matricielle :

$$[Z(k)]\,q(p) = -[C(k)]\,\theta$$

où $Z(k)$ est la matrice d'impédance du système qui s'écrit :

$$[Z(k)] = \left\{-[\mu]\omega^2 + [\gamma] + 1/2\,\rho V^2 [A(k) + i B(k)]\right\}$$

dans une base de modes propres, μ et γ (respectivement matrice des masses et des rigidités généralisées) sont diagonales. $C(k)$, $A(k)$ et $B(k)$ sont les parties réelles et imaginaires des forces aérodynamiques instationnaires dues à un mouvement de l'aileron $(C(k))$ ou à un mouvement de l'aile $[A(k)$ et $B(k)]$

On en tire : $q = -[Z^{-1}][C]\,\theta$

et $[\bar{w}][q] = -[\bar{w}][Z]^{-1}[C]\,\theta$

$\bar{w}$ est la matrice des modes propres sans vent au 1/4 avant de la tranche d'aile en face de la surface de contrôle.

En posant $z = |\bar{W}|\,|q|$

on a : $\frac{z}{\theta} = -|\bar{W}|\,[Z_{(k)}]^{-1}|C_{(k)}| = T_{(S)}$

$C_{(k)}$ est la colonne des forces induites sur l'aile par la surface de contrôle, la partie aérodynamique de ces forces s'écrit :

$$C_{(k)} = K.\rho V^2 \begin{bmatrix} \delta_1 & \gamma_1 & 0 \\ \delta_2 & \gamma_2 & 0 \\ 0 & 0 & 1 \end{bmatrix} \begin{bmatrix} 0 & 0 & k_d \\ 0 & 0 & m_d \\ 0 & 0 & n_d \end{bmatrix} \begin{bmatrix} \delta_1 & \delta_2 & 0 \\ \gamma_1 & \gamma_2 & 0 \\ 0 & 0 & 1 \end{bmatrix} = \begin{bmatrix} C_1 \\ C_2 \end{bmatrix}$$

La partie relative aux forces d'inertie de la gouverne a été négligée après un calcul préliminaire comparatif.

La fonction $T_{(S)}$ a été calculée pour 200 valeurs de fréquence dans la gamme 0,20 Hz. Les forces aérodynamiques des fonctions A, B, C ont été interpolées pour chaque fréquence réduite à partir du calcul exact effectué pour 7 valeurs discrètes de k (L'interpolation est du type parabolique) :

$$\Theta = K_2 \left[\delta_{c1}\ \delta_{c2} \ldots \right] q$$

δ_i γ_i sont les amplitudes des déplacements du point de la tranche d'aile comportant la gouverne de contrôle et situé au quart avant de celle-ci. Les déplacements étant considérés dans les six modes introduits dans le calcul (sans vent).

δ_{c1} δ_{c2} sont les déplacements du point de contrôle dans le vent (point 86, Fig. 1).

En boucle ouverte on peut écrire pour le système avec contrôle :

$$T_{O.L} = -\omega^2 T_S T_C$$

où T_C est la fonction de transfert de la loi de contrôle et $T_{CL} = \frac{-\omega^2 T_S T_C}{1 - \omega^2 T_S T_C}$ en boucle fermée.

La fonction T_C s'écrit :

$$T_C = \pm G_3 T_1 T_3 (G_1 + G_2 T_2) T_4 \text{ radian/m/s}^2$$

avec T_1 = filtre de bande pour limiter le nombre de modes à contrôler :

$$T_1 = \frac{1}{1 + 0{,}8105S + 0{,}0001759S^2} \times \frac{1}{1 + 0{,}0245S + 0{,}0001759S^2} \times \frac{0{,}07958S}{1 + 0{,}07958S}$$

est un pseudo-intégrateur qui coupe les fréquences basses :

$$T_2 = \frac{0{,}282S}{1 + 0{,}282S + 0{,}212S^2}$$

T_3 est la fonction de transfert du vérin et de la servo-valve fournis par l'USAF

$$G_1 = 0{,}1 \qquad G_2 = G_3 = 1$$

Le schéma bloc de la figure 4 montre le principe de la loi de contrôle. Par ajustement des gains G_1 et G_2 la phase globale de la fonction de transfert T_C est égale à 180° à la fréquence critique de 6 Hz du mode à contrôler. La réinjection des forces sur l'aile est alors une rigidité pure et négative, compte tenu des hypothèses suivantes introduites dans le calcul :

- les forces aérodynamiques induites par la gouverne de contrôle n'agissent de façon sensible que dans la tranche d'aile où est située cette gouverne ;
- les parties réelles des forces aérodynamiques créées par cette gouverne dépendent peu de la fréquence réduite $k = \frac{\omega L}{V}$ dans un intervalle de quelques Hertz (de 5 à 10 Hertz par exemple) ;
- les parties imaginaires des forces aérodynamiques sont faibles devant les parties réelles en sorte que le déphasage qu'elles introduisent peut être négligé.

Ces différentes hypothèses ont été vérifiées par des essais en soufflerie dans lesquels on mesurait les champs de pression instationnaire créés par une gouverne excitée harmoniquement à différentes fréquences.

(La forme en plan des maquettes qui ont servi à ces mesures était voisine de celle de l'aile de l'avion F17).

Il résulte de ces hypothèses que les forces induites par la gouverne sont pratiquement en phase avec le mouvement de celle-ci et donc (suivant le signe choisi) en phase ou en opposition avec le mouvement du point de contrôle.

D'où l'effet de rigidité négative qui a été utilisé et qui tend à abaisser la fréquence du mode de flexion en réduisant l'importance des termes de couplage par séparation des fréquences critiques et tend donc à réduire les risques de flottement.

b.2) Comparaison des résultats d'essais avec la théorie - Cas avec contrôle

Les valeurs expérimentales des amortissements et des fréquences des modes intervenant dans le phénomène de flottement ont été obtenues expérimentalement en analysant les courbes de densité spectrale pour différents capteurs.

Une tentative d'interprétation faite avec la "Peak Hold Method" (enveloppe des valeurs maximales pour chaque fréquence des courbes de densité spectrale) a fait apparaître une large dispersion des amortissements. Ceci peut être dû aux raisons suivantes :

- les valeurs maximales au cours du temps de la courbe de densité spectrale dépendent de deux paramètres d'entrée :
  - du niveau de turbulence de la soufflerie, qui est fonction de la pression génératrice et du nombre de Mach ;
  - de l'amortissement global du système (aérodynamique + structural) qui est le seul qui doit être considéré ;

  Le premier paramètre étant ni constant, ni connu, fausse la mesure, d'autant plus que l'on veut procéder à une extrapolation sur de faibles valeurs d'amortissement pour obtenir le point de flottement.
- enfin, la fonction inverse du maximum de la courbe de densité spectrale est une fonction inconnue, non linéaire en général, qu'il est difficile d'extrapoler.

La figure 5 présente le calcul avec contrôle, elle doit être comparée à la figure 2 (calcul sans contrôle).

La comparaison des résultats d'essais et de calcul avec contrôle est portée sur la figure 6.

On peut noter l'accord correct qui existe quant à l'allure des courbes théoriques et expérimentales.

L'explositivé du phénomène est la même dans les deux cas et a été considérablement réduite par rapport au cas nominal sans contrôle. La limite de la pression dynamique que l'on pourrait atteindre en augmentant encore la pression dynamique ne présente pas un grand intérêt si on considère que la courbe d'amortissement du mode critique est maintenant très plate. On rencontrerait une entrée en flottement très progressive et donc mal définie.

Il faut remarquer sur la courbe des fréquences que l'effet recherché d'introduction d'une rigidité négative sur le mode de flexion est similaire en calcul et en essais.

L'amortissement de structure a été soustrait des courbes d'amortissements présentées, elles ne comportent donc que la partie d'aérodynamique instationnaire.

c) Amélioration de la loi de contrôle

A partir de ces résultats on peut avoir une confiance raisonnable dans le calcul des forces aérodynamiques agissant sur l'aile et la gouverne de contrôle. Une optimisation de la loi de contrôle peut alors être appliquée.

L'amélioration a été obtenue par un calcul a posteriori en réduisant la variation de phase en fonction de la fréquence dans la fonction T_S relative à la loi de contrôle.

Le calcul a été effectué à partie d'une loi idéale dont le module serait constant et égal à un radian de rotation de la gouverne pour 1 mètre de déplacement du point de contrôle et en prenant d'autre part des pentes de variations de phase en fonction de la fréquence égales à :

1) $\frac{\partial \varphi}{\partial f} = 0°/Hz$ phase constamment nulle ou égale à 180°

2) $\frac{\partial \varphi}{\partial f} = -7{,}5°\ Hz$ phase variant linéairement avec la fréquence

3) $\frac{\partial \varphi}{\partial f} = -15°/Hz$

4) $\frac{\partial \varphi}{\partial f} = -20°/Hz$

Dans tous les cas 1) 2) 3) et 4) la phase est calée égale à 180° pour la fréquence critique de 6 Hertz.

Les courbes d'évolution de fréquences et d'amortissement pour les différents cas de contrôle sont données pour les modes de flexion (mode n° 2) et de tangage engin (mode n° 3). Bien entendu le calcul complet à six modes a été effectué.

On voit que pour $\frac{\partial \varphi}{\partial f} = 0°$ (phase nulle dans toute la bande de fréquence) il n'existe plus de possibilité de flottement, les modes de structures ne sont jamais couplés, les résultats de calcul sont identiques à ceux que l'on pourrait obtenir en faisant le calcul mode par mode (calcul à 1 degré de liberté).

Lorsque la pente de phase atteint -20°/Hz on se retrouve pratiquement dans les conditions de l'essai et le flottement réapparaît avec un gain sur la pression dynamique de 60% dû au contrôle.

CONCLUSION

On a pu, dans cette étude, valider dans une première phase les hypothèses restrictives dans le calcul des forces aérodynamiques instationnaires aussi bien en ce qui concerne les termes relatifs à l'aile que ceux afférents à la surface de contrôle.

La loi utilisée pour réduire le flottement, consistant à introduire un terme de rigidité sur l'un des modes de la structure, s'est avérée correcte. La comparaison théorie-expérience est en bonne concordance.

Il est ensuite facile, partant d'une fonction de transfert connue pour la loi de contrôle, de l'améliorer par le calcul en réduisant la pente de la courbe de phase fonction de la fréquence.

Toutefois, cette méthode ne s'attache pas à obtenir une optimisation sur les marges de gain ou de phase du contrôle en fonction de paramètres comme la pression dynamique ou le nombre de Mach.

Une loi de contrôle numérique pilotée par ces mêmes paramètres s'avèrera nécessaire dans le futur pour des applications portant sur des avions.

BIBLIOGRAPHIE

[1] HWANG C., JOHNSON E.H., MILLS G.R., NOLL T.F., FARMER M.G.
Wind tunnel test of a fighter aircraft - Wing/store flutter suppression system - An International effort - 50th Meeting of the SMP of AGARD, 13-18 April 1980, Athens, Grece.

[2] DESTUYNDER R., HÖNLINGER H.
Active control technology for flutter suppression - V.K.I. Lecture Series - 4-8 Dec. 1978, Brussels/Belgium.

[3] SENSBURG O., HÖNLINGER H., NULL T.E.
Active flutter suppression on a F4F Aircraft with external stores using already existing control surfaces - 21th Structures, Structural Dynamics and Materials Conference of the AIAA, 12-14 May 1980, Seattle (Was.) USA.

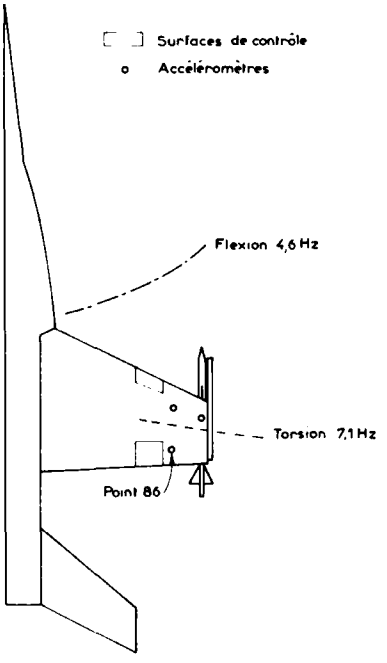

Fig. 1 – F17 maquette. Configuration B.

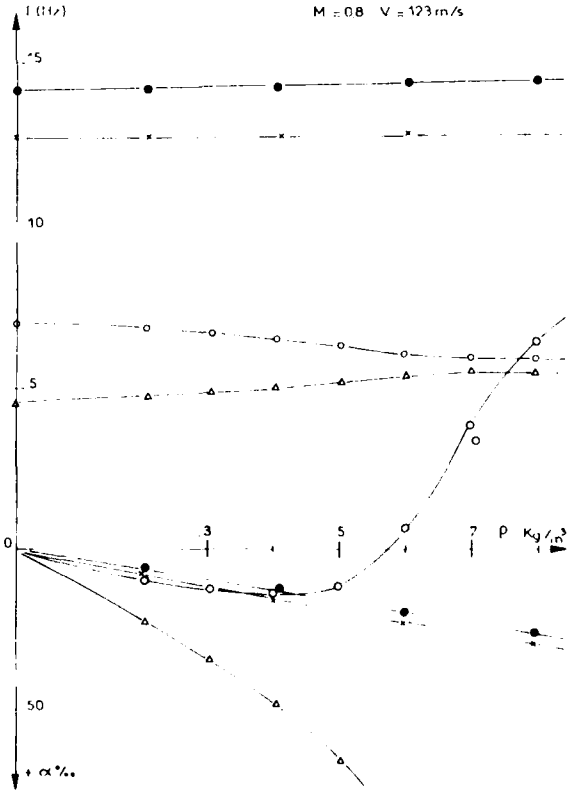

Fig. 2 – F17 maquette de flottement. Théorie sans contrôle.

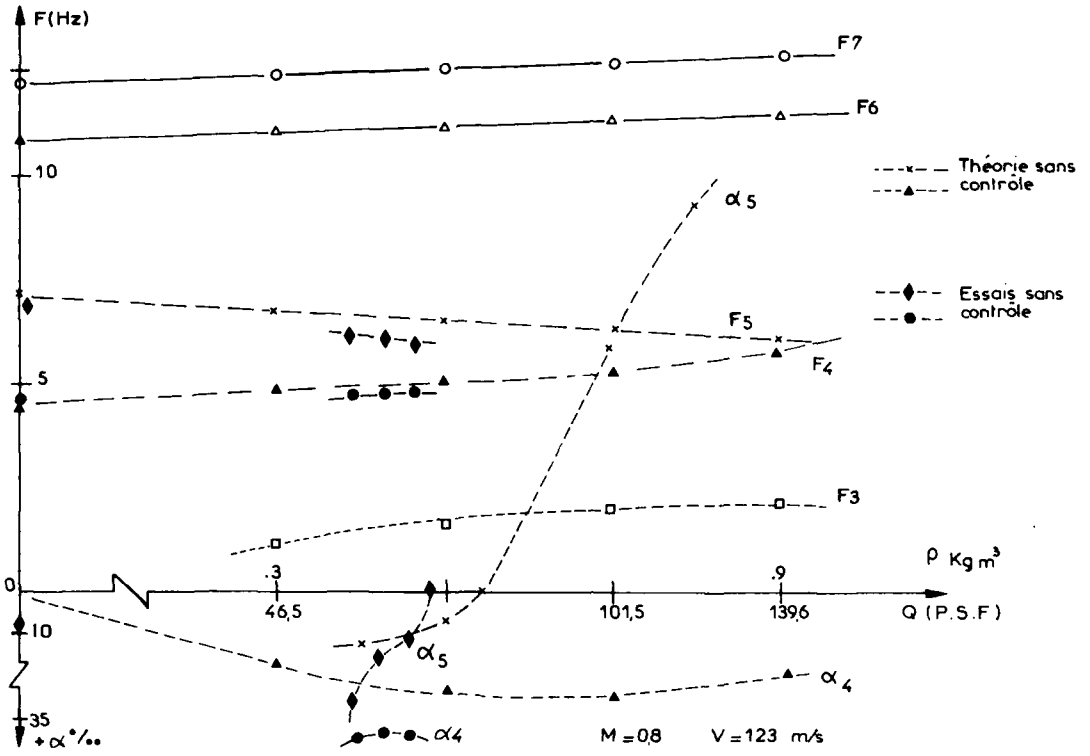

Fig. 3 – F17. Comparaison essais-calculs sans contrôle.

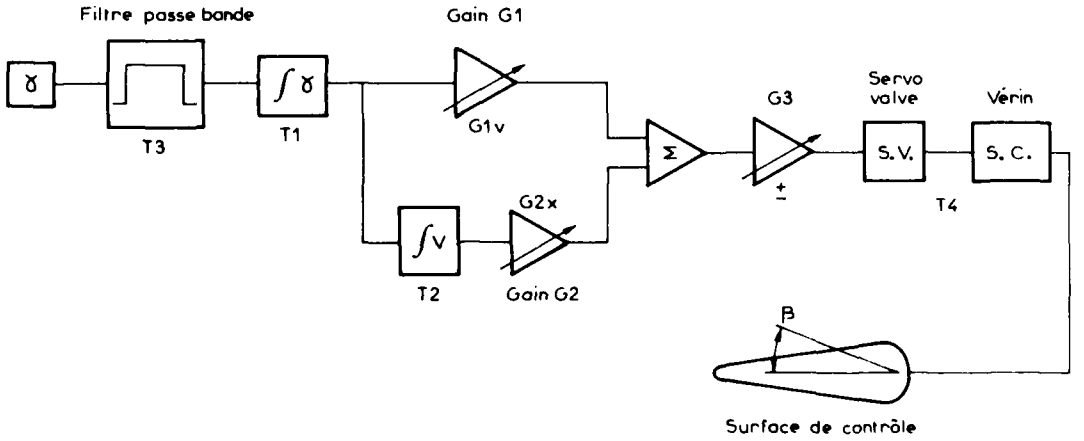

T3 T1 (G1+G2 T2) G3 T4

Fig. 4 – Bloc diagramme de la loi de contrôle.

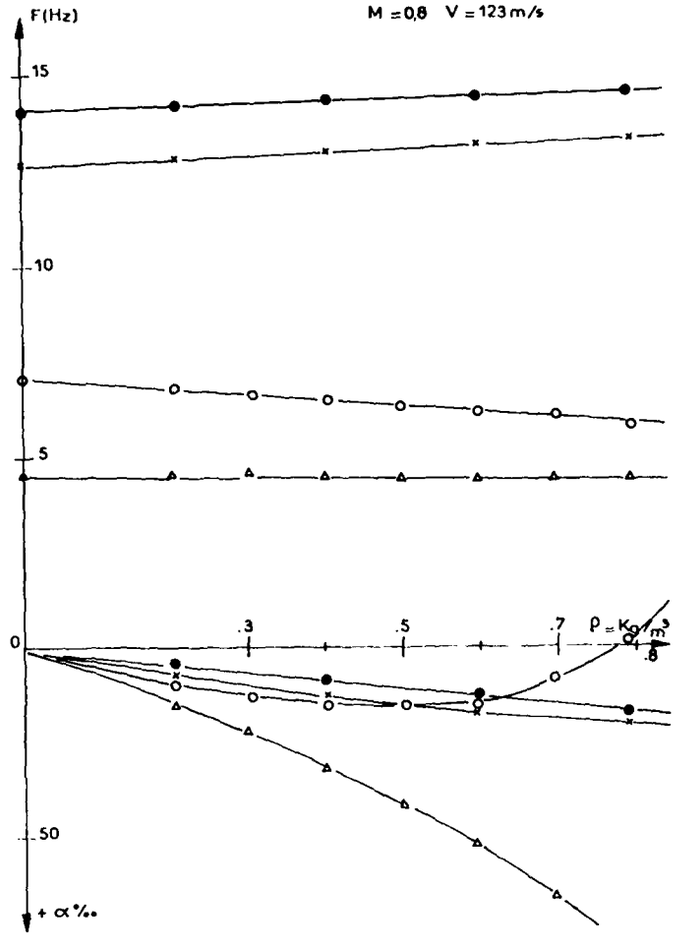

Fig. 5 – F17 maquette de flottement. Théorie avec contrôle.

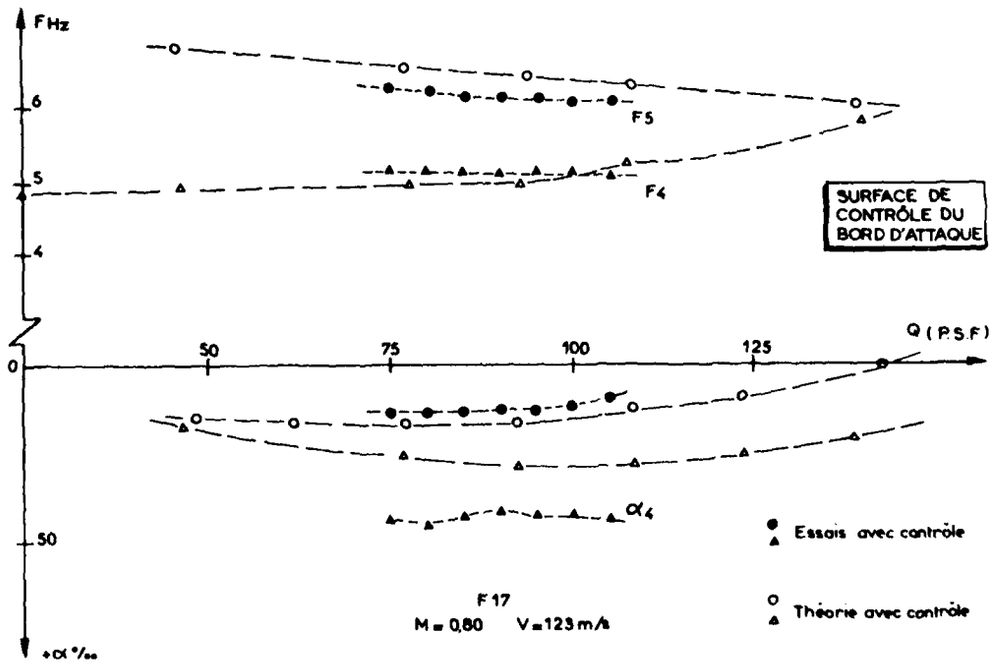

Fig. 6 Comparaison essais-calculs avec loi de contrôle

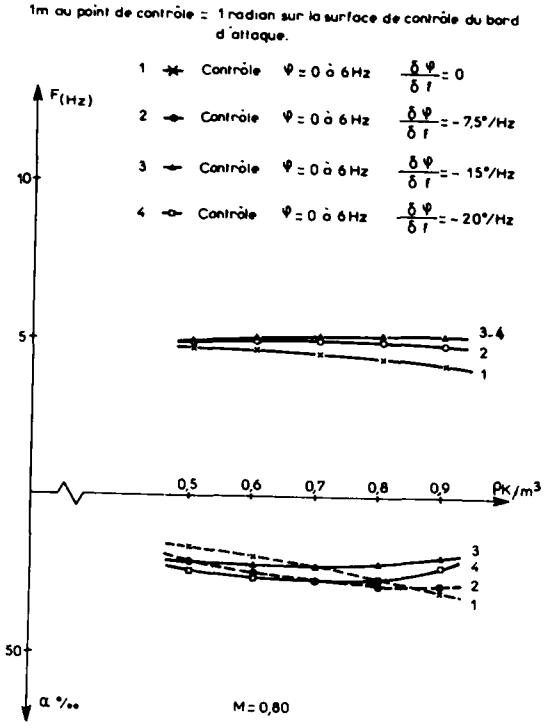

Fig. 7 – F17. Théorie 6 modes CCV F17. Mode No 2.

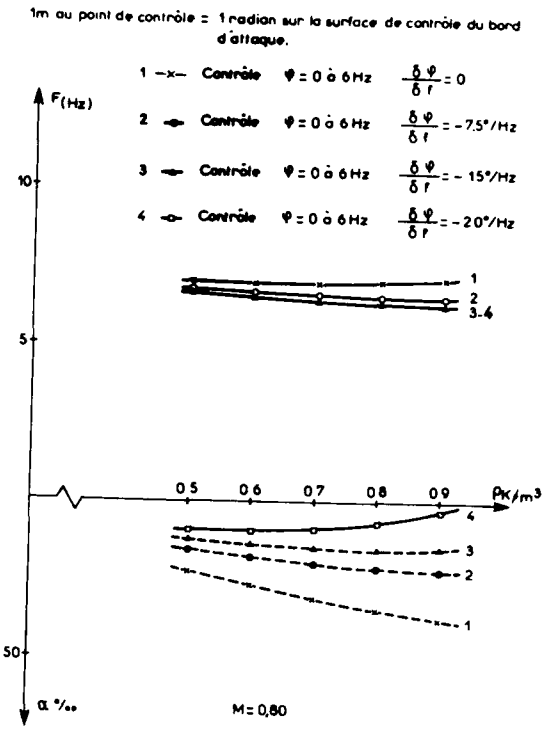

Fig. 8 – F17. Théorie 6 modes. CCV F17. Mode No 3.

WIND TUNNEL TESTS ON A FIGHTER AIRCRAFT WING/STORE FLUTTER SUPPRESSION SYSTEM - THE B.Ae CONTROL LAW

by

M. R. TURNER

British Aerospace, Aircraft Group

Weybridge/Bristol Division

Filton, P.O. Box 77, Bristol BS99 7AR, U.K.

SUMMARY

A B.Ae control law designed using analytical data was tested on a model of the YF-17 in the NASA Langley 16' wind tunnel and succeeded in meeting the requirement to increase the flutter dynamic pressure by 70% at M = 0.8.

Because the store configuration chosen for these tests produced a flutter mechanism which was both hard and near to classical frequency coalescence, it was necessary to use a multiple output control law to achieve the stability margin objectives of $\mp 60^{o}$ and ∓ 6dB.

The B.Ae control law was designed using a novel procedure which provides these stability margins, uses minimum control surface movement in turbulence and can be designed using either analytical or empirical data. Two wing tip accelerometers and a leading edge control surface were used.

Empirical open loop transfer functions obtained during the test showed that the analytical data overestimated the response of the flutter mode to leading edge control surface excitation.

1. INTRODUCTION

The United States Air Force Flight Dynamics Laboratory (AFFDL) sponsored the design, construction and wind tunnel testing of a YF-17 model to demonstrate active control of store flutter.

Northrop Corporation were contracted to design the model and the active flutter control laws, and to test these in the 16' Transonic Dynamics Tunnel of NASA Langley Research Centre.

After an initial phase of wind tunnel testing (ref. 1), information exchange agreements were drawn up between the AFFDL and each of three European countries (U.K., Germany and France) whereby active flutter control laws would be designed in each of these three countries for the YF-17 model to be tested along with control laws designed by Northrop.

These control laws were tested in October 1979 (ref. 2) and this report briefly describes the work done by British Aerospace. It is in three parts: the basic properties of the model as shown by analytical studies, control law design and the results of the wind tunnel testing.

2. WIND TUNNEL MODEL

Fig. 1 shows the 30% scale wind tunnel half model. It is supported vertically by soft springs and attached to the tunnel wall by roll bars so that only symmetric motion of the aircraft is represented. The wing and fuselage structure is dynamically representative of the full scale aircraft.

Two control surfaces (one leading edge and one trailing edge) are available for active flutter control. Each is moved independently by its own hydraulic actuator.

For the October 1979 tests, there were four accelerometers on the outer wing available for active flutter control. Also the model had a pylon mounted AIM-7S missile and an empty wing tip launcher rail (i.e. store configuration B).

3. DESIGN OBJECTIVE

The design objective laid down by the AFFDL was to increase the flutter dynamic pressure by 70% with stability margins of $\pm 60^{\circ}$ and ∓ 6dB using the existing control surfaces and accelerometers.

4. BASIC PROPERTIES OF THE MODEL

The analytical studies on the wind tunnel model were made using two sets of aeroelastic data provided by the AFFDL and Northrop Corporation. The first (a 10 degrees of freedom system) was based upon seven calculated normal modes of the model. The second (a 13 degrees of freedom system) was produced later and was based upon ten GVT modes modified to give agreement with the critical flutter dynamic pressure (QF) measured in earlier wind tunnel tests (ref. 1).

4.1 Flutter Curves

Fig. 2 shows the basic flutter curves for the 10 d. of f. system. The flutter root is that associated with the air off fundamental wing torsion mode. Below the flutter dynamic pressure (QF) the flutter root damping does not exceed 1% critical. However, above QF the damping falls rapidly to about -10% critical at 1.7QF i.e. the flutter is hard.

Fig. 3 shows the flutter curves for the binary system consisting of the fundamental bending and torsion modes. The frequency and damping curves are identical to those of the corresponding roots in fig. 2 with an almost identical QF. This shows that the flutter mechanism is pure binary.

Also shown in fig. 3 is the effect of ignoring the out of phase aerodynamic generalised forces ($[B] = [0]$). This shows the classical frequency coalescence flutter (ref. 3 and 4) with the flutter speed not very much changed.

Therefore fig. 2 and 3 show that we are attempting to perform active flutter control of hard, near frequency coalescence, binary flutter.

4.2 Open Loop Transfer Functions

4.2.1 Input to the Leading Edge Control Surface Actuator

Fig. 4 shows the open loop transfer function (o.l.t.f.) at 1.7QF for input to the leading edge control surface actuator and velocity output from the outboard aft (O/A) accelerometer position computed using the 10 d. of f. system data.

There are two significant features which were seen from the o.l.t.f. for outputs at 100 positions over the wing surface. These were: all anticlockwise lobes are narrow and have the same mean phase angle, and the wing tip transducers sense the least response in the modes not involved in the binary flutter.

This means that a simple control law using a single transducer will have inadequate phase margins, and a control law which uses the two outboard transducers will have least problems avoiding closed loop instability.

4.2.2 Explanation of Open Loop Transfer Function Properties

Fig. 5 and ref. 5 show that if the dynamic system is simplified to:

a binary flutter system without out of phase aerodynamics

excited by only the in phase aerodynamics of a control surface,

the o.l.t.f. between the control surface angle β and the displacement anywhere on the structure w is the product of two transfer functions each of which has real values for all frequencies.

As a result, the velocity o.l.t.f. $\dot{w}/\beta$ will have values only on the imaginary axis, starting and finishing at the origin. This means that a single input/single output control law for such a system will have zero phase margins.

Fig. 6 shows what happens when the YF-17 model is represented in this simplified manner. The velocity output at O/A due to the leading edge control surface motion gives an o.l.t.f. which travels up then down the positive imaginary axis as frequency increases. However, when the trailing edge control is used, the o.l.t.f. has values along both the positive and negative halves of the imaginary axis. This causes a significant difference between the leading edge and trailing edge o.l.t.f. when the out of phase aerodynamics are included in the binary flutter mechanism (i.e. $[B] \neq [0]$). This is shown on the right hand side of figure 6.

It shows that if the out of phase control surface aerodynamics are ignored, active flutter control can be achieved using the leading edge control driven by displacement (or acceleration) output at O/A, but only with poor phase margins. On the other hand, using the trailing edge control with velocity feedback from O/A will give excellent phase margins.

However, when the control surface out of phase aerodynamics are included, the leading edge control o.l.t.f. is almost unchanged but the trailing edge control o.l.t.f. loses almost all of its potential phase margin (ref. 5).

5. CONTROL LAW DESIGN

Ref. 6 and 7 show by analytical studies that the stability margins specified in section 3 can often be achieved with a simple control law using a single transducer and a single control surface. This is done by careful choice of the transducer position. However, section 4 reports that the phase margin requirements ($\mp 60^{\circ}$) of the YF-17 Design Objectives cannot be achieved using a single transducer with either the leading edge or trailing edge control surface (see also ref. 8). Therefore a multiple output control law is required.

5.1 Optimal Control Theory

An analytical control law which satisfies the Design Objectives, and does so using minimum control surface motion in tunnel turbulence, can be derived from Optimal Control Theory. This is fully described in references 6 and 9 and outlined in figure 7.

The theoretical derivation follows recognition that the Matrix Riccati Equation for solving the Linear Optimal Regulator Problem can be put into Pole Placement form. Then letting the state weighting matrix $[Q]$ in the cost function be zero leads to the simple criterion: the control law allows the closed loop poles to be the same as the open loop poles except that the real part of the unstable open loop poles change sign. This means that the Nyquist Plot will consist only of an anticlockwise circle with its centre at -1,0 and of unit radius, for every unstable root. In other words, the feedback signal contains only flutter mode velocity (fig. 8).

However, this control law formally requires the sensing of all the system states (e.g. 20 states for 10 second order degrees of freedom) and the feedback signal to be a weighted sum of these states. This is obviously not practical.

Fortunately, for this configuration of the YF-17 model the flutter mechanism is a pure binary fairly well separated in frequency from adjacent roots. Therefore, the control law can be designed for the flutter binary and be expressed as the weighted sum of the displacement and velocity output at two transducer positions with a correcting filter to allow for the actuator transfer function (fig. 9).

Such a control law was designed by Pole Placement computation for the YF-17 model at 1.7QF using the output of the two outboard transducers. The resulting Nyquist Plot for the 10 d.of f. system with this control law is shown in figure 10. It gives the required circular anticlockwise lobe and good stability margins at all frequencies.

5.2 A Practical Control Law Design Procedure

However, a more practical approach can be made by direct use of the known desirable anticlockwise circular Nyquist Plot. That is to take the four component o.l.t.f. (i.e. velocity and displacement outputs for two transducer positions) and find the four gains required to combine them to give a least squares fit to the perfect circle. In this way the actuator transfer function can be included in the basic o.l.t.f., significant response in adjacent modes over the flutter root bandwidth can be allowed for, and empirical o.l.t.f. can be used if necessary.

Fig. 11 shows the results of doing this using the two outboard accelerometers and including the actuator transfer function. Partial integration of the accelerometer outputs is used to avoid non zero response at zero frequency. The results are good. The flutter lobe fits the desired circle well enough and the only significant open loop stable mode which is threatened by closed loop instability is the calculated 38 Hz wing tip launcher rail fundamental bending mode. However, the aerodynamic damping in this mode is only 0.1% critical and structural damping (not included in these calculations) will enormously attenuate this lobe.

A notch filter can then provide any further attenuation necessary.

Fig. 12 shows the stability margins between QF and 2.6QF for the control law designed at 1.7QF shown in fig. 11. These stability margins are excellent and close to those of the Design Objectives. The block diagram for this control law is the upper horizontal path of fig. 15. This will be referred to as the four gains, two transducers (4G/2T) control law.

5.3 Effect of 4G/2T Control Law on Flutter Aerodynamic Coefficients

Any active flutter control law can be thought of as effectively causing a change to the flutter generalised force coefficients. To investigate this, the 4G/2T control law was designed for the flutter binary of the YF-17 model at 1.7QF using the leading and trailing edge control surfaces in turn.

Although all eight generalised aerodynamic force coefficients were effectively changed, the major effects were:

(a) leading edge control surface:

- 0.2	×	work done on	torsion	mode	by	in phase		bending	mode	aerodynamics
2	×	"	"	"	"	"	" out of phase	"	"	"
0.7	×	"	"	"	"	"	" in phase	torsion	"	"
5	×	"	"	"	"	"	" out of phase	"	"	"

(b) trailing edge control surface:

-0.3	×	work done on	bending	mode	by	in phase		torsion	mode	aerodynamics
2	×	"	"	"	"	"	" out of phase	"	"	"
2	×	"	"	"	"	"	" in phase	bending	mode	aerodynamics
5	×	"	"	"	"	"	" out of phase	"	"	"

This shows that the leading and trailing edge control surfaces do work primarily on the torsion and bending modes respectively. The main stabilising effect comes from changing the sign of a cross aerodynamic stiffness while the other changes provide the required stability margins (ref. 5).

6. FURTHER CONTROL LAW DESIGN

6.1 Analytical Studies using Later Data

The work described so far (ref. 9) has been done using the earlier analytical data (10 d of f system) which included seven calculated structural modes. This work was repeated (ref. 10) using later data (13 d.of f. system) which included 10 GVT modes.

Fig. 13 shows the deflections over the wing in these 10 structural modes. The first two are the fundamental bending and torsion modes of the flutter binary.

Fig. 14 compares the o.l.t.f. for input to the leading edge control surface actuator and velocity output from the outboard accelerometer positions at 1.7QF. For both sets of data the potential phase margins for single output control law are inadequate.

6.2 Extra Feedback Filters Defined by Northrop

From their experience in earlier tests (ref. 1) Northrop stated that extra filters were required to avoid closed loop instabilities at frequencies well separated from the flutter root bandwidth. These are two notch filters (34 and 90 Hz) and a second order low pass filter (42 Hz cutoff) to protect high frequency roots, and two high pass filters (5.3 and 1.6 Hz cutoff) to avoid rigid body instability (fig. 15 and 16).

To study the effect of these filters, as well as the leading edge control surface actuator, the single output o.l.t.f. for the outboard accelerometer positions and the Nyquist Plots for the 4G/2T control laws were produced for the six filter combinations tabulated in fig. 16.

Fig. 17 shows the attentuation and phase lag produced by each filter combination at the 1.7QF flutter root frequency.

Fig. 18 shows the effect of these filter combinations on the anticlockwise lobe of the o.l.t.f. for leading edge control surface input and displacement output at O/A. Whereas the mean phase of the lobe varies with filter combination as would be expected from fig. 17, the potential gain and phase margins for a single output control law reduces dramatically as the number of filters increases such that for FC6 (the filter combination used eventually in the wind tunnel test) they are only $\mp$ 1.3 and $\mp 4^{\circ}$.

Fig. 19 shows the effect of each filter combination on the flutter lobe of the 4G/2T control law Nyquist Plot at the Design Condition of 1.7QF. Shown dashed on each flutter lobe is the ideal circle of unit radius and with centre at -1,0.

Although the circle fit is not very good after FC1 and FC2, the stability margins are excellent for all filter combinations.

The four feedback gains (J1 to J4) were calculated by the least squares fit procedure described in section 5.2 for each of the six filter combinations as shown in figure 20.

Fig. 21 shows the closed loop flutter curves for the control law for FC5 designed at 1.7QF. For clarity, only the roots of the first two structural modes (i.e. the flutter binary) are shown. They show no tendency towards closed loop instability. Also, a Nyquist Plot study showed the same for the other roots.

Section 5.1 suggested that the frequency of the first two roots would not change as the feedback gain increased. Fig. 22 shows that this is true for the flutter root but not for the first root. This is because the filters prevent the anticlockwise lobe for FC5 in fig. 19 from being a perfect circle (as it is for FC1) so that there is significant feedback of first mode response.

Because it is only the filter properties over the flutter root frequency bandwidth which affect the value of the four gains and the flutter root stability margins, it would be much better to design a bandpass filter which introduces the minimum of phase and amplitude change over this bandwidth while providing the required amount of attenuation and phase change at the lower and higher frequencies where closed loop instabilities may be introduced. This, of course, would require an accurate definition of the attenuation and phase requirements to avoid closed loop instabilities.

7. WIND TUNNEL TEST RESULTS

During the wind tunnel tests in October 1979, the AFFDL Design Objective was reduced to increasing the flutter dynamic pressure by 70% without any requirement to demonstrate stability margins.

It had been expected that the analytical control law would not be adequate to provide the required stability margins in the test. It had therefore been planned to obtain empirical o.l.t.f. and use the least squares fit procedure on these to produce empirical 4G/2T control laws.

However, the 70% increase in flutter dynamic pressure was achieved using the law calculated using the 13 d. of f. analytical data for the additional filters that Northrop considered necessary i.e. filter combination 6 (fig. 16).

As the tests proceeded in dynamic pressure, the stability margins were partially checked by reducing the control law overall gain down to 0.7 of its nominal value and also introducing up to 30° phase lag at the flutter root frequency by means of an all pass filter. Resulting from this, the control law was tested at 1.7QF with only 0.9 and 0.8 of the nominal gain and with no phase lag. This was because the tests at lower dynamic pressure had predicted that at 1.7QF: the flutter root would not be stable for 0.7 of nominal gain; and for nominal gain, with or without any phase lag, the model response to tunnel turbulence in the Pylon Side Bending Mode at about 13 Hz would cause motion of the leading edge control surface which could damage the actuator.

Because of this response to tunnel turbulence, it was not possible to obtain good empirical o.l.t.f. above 1.2QF (90 p.s.f.). However, from the comparison of the analytical and empirical o.l.t.f. at 1.2QF it was possible to obtain empirical correction factors for the analytical data concerning the flutter and 13 Hz lobes (ref. 11).

The effect of applying these correction factors to the analytical Nyquist Plot at 1.7QF is shown in fig. 23. The flutter lobe is reduced by a factor of 0.7; the 13 Hz lobe is increased by a factor of 2 and has a 60° phase lead relative to the negative real axis.

This change to the analytical Nyquist Plot makes it consistent with the test results which limited the 1.7QF tests to 0.9 and 0.8 times the nominal gain.

Given this information, it appears that good empirical o.l.t.f. could be obtained at 1.7QF by merely introducing a notch filter into the control law to prevent the large control surface response to tunnel turbulence. Then these o.l.t.f. could be used to design a control law with good stability margins.

8. CONCLUDING REMARKS

The YF-17 model tested had extreme flutter characteristics which caused a new control law design procedure to be developed to obtain good stability margins. This procedure gave a control law, based upon analytical data and a leading edge control surface, which was robust enough to achieve the required 70% increase in flutter dynamic pressure.

It could be that when designing for active flutter control of an aircraft, the analytical data is not adequate so that good quality empirical data may be necessary. Also, only a trailing edge control surface may be available.

Therefore, the following work on the YF-17 model would be useful.

(1) Analytical studies to find the relative effectiveness of the leading and trailing edge control surfaces for active flutter control.

(2) Wind tunnel tests to achieve 1.7QF using a control law based upon analytical data and the trailing edge control surface.

(3) Wind tunnel tests designed to obtain good quality open loop transfer functions by separately exciting with the leading and trailing edge control surfaces up to 1.7QF.

(4) Wind tunnel tests of control laws based upon the empirical data of (3) above.

9. REFERENCES

1. C. HWANG, B. A. WINTHER, G. R. MILLS
"Demonstration of Active Wing/Store Flutter Suppression Systems"
AFFDL Report TR-78-65 June 1978

2. C. HWANG, E. H. JOHNSON, G. R. MILLS, T. E. NOLL, M. G. FARMER,
"Wind Tunnel Tests of a Fighter Aircraft Wing/Store Flutter Suppression System - an International Effort"
Paper presented at 51st SMP of AGARD Athens April, 1980

3. T. von KARMAN, M. A. BIOT
"Mathematical Methods in Engineering"
McGraw - Hill Book Company 1940

4. S. PINES
"An Elementary Explanation of the Flutter Mechanism"
Paper presented at National Specialists Meeting on Dynamics and Aeroelasticity
Fort Worth Texas 1958

5. M. R. TURNER, N. F. MATTOCK
"Active Control of Near Frequency Coalescence Flutter"
B.Ae Report B.Ae/WBD/D/RD/112 July, 1980

6. M. R. TURNER
"Active Flutter Suppression"
AGARD-CP-175 Brussels April, 1975

7. M. R. TURNER, N. F. MATTOCK
"Active Flutter Control"
B.Ae Report B.Ae/WBD/D/RD/106 September, 1978

8. M. R. TURNER, C. G. LODGE
"A Practical Optimum Selection Procedure for a Motivator in Active Flutter Suppression System Design on an Aircraft with Underwing Stores"
AGARD-CP-228 Lisbon April, 1977

9. M. R. TURNER, N. F. MATTOCK
"Active Flutter Control of a Wind Tunnel Model of the YF-17 with Store Configuration B"
B.Ae Report B.Ae/WBD/D/RD/108 March, 1979

10. M. R. TURNER, N. F. MATTOCK
"Active Flutter Control of a Wind Tunnel Model of the YF-17 with Store Configuration B - Part 2"
B.Ae Report B.Ae/WBD/D/RD/109 October, 1979

11. M. R. TURNER, J. C. COPLEY, C. W. SKINGLE
"Active Flutter Control Test on a YF-17 Model - Preliminary Observations on Performance of B.Ae Control Law"
B.Ae/WBD/D/RD/111 October, 1979

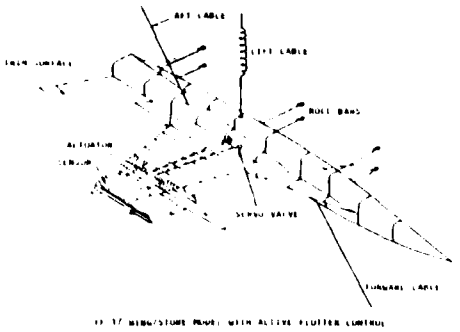

FIG.1

FIG.4

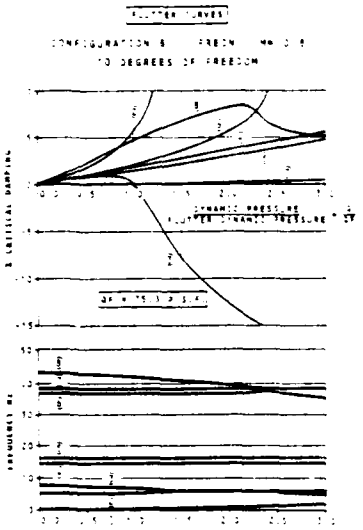

FIG.2

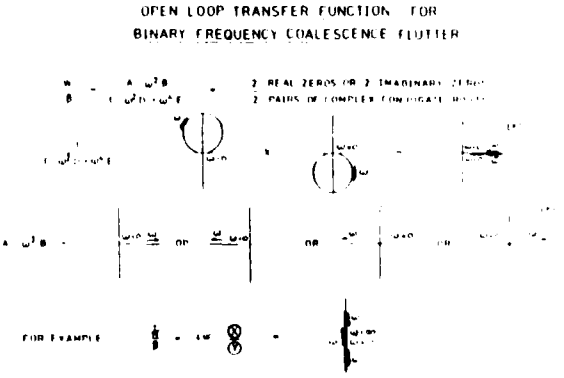

FIG.5

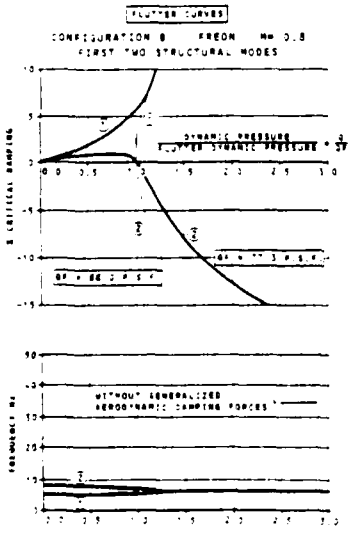

FIG.3

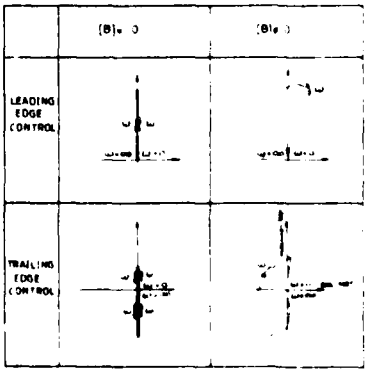

FIG.6

AN [IDEAL STABILISING SINGLE INPUT CONTROL LAW]
OF THE FORM [$u = -\underline{k}_1 \{x\}$] CAN BE FOUND FOR
AN UNSTABLE SYSTEM [$\{\dot{x}\} = [S]\{x\} + \{B\}u$]
BY FINDING $\underline{k}_1$ WHICH MINIMISES [$J = \int_0^{\infty} (\{x\}^T [Q] \{x\} + ru^2)\, dt$]
USING THE [MATRIX RICCATI EQUATION] WHICH CAN BE PUT
INTO [POLE PLACEMENT] FORM.

- MINIMISING J ENSURES STABILITY
- FOR [$[Q] = 0$]:
  - (1) R.M.S OF u IN CONTINUOUS RANDOM EXCITATION IS MINIMISED
  - (2) CLOSED LOOP POLES = OPEN LOOP POLES EXCEPT REAL PART OF UNSTABLE POLES CHANGE SIGN.

FIG.7

NYQUIST PLOT AT 1.7QF

INPUT: $\delta_{L.E.}$ ACTUATOR
OUTPUT: J_1MO/F + J_2MO/F + J_3MO/A + J_4MO/A
ACTUATOR TRANSFER FUNCTION = UNITY
$J_1 \rightarrow J_4$ FROM POLE PLACEMENT CALCULATION ON FLUTTER BINARY

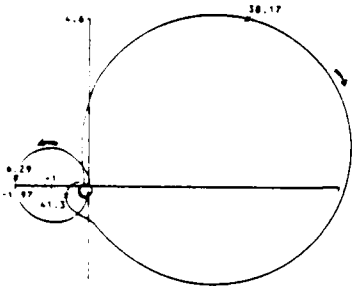

FIG.10

IDEAL CONTROL LAW

$u = k\, \underline{k}_1 \{x\}$
$\underline{k}_1$ = IDEAL CONTROL LAW FEEDBACK GAINS
k = OVERALL GAIN FACTOR

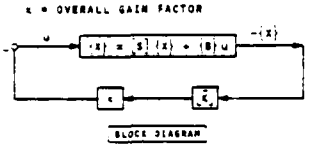

BLOCK DIAGRAM

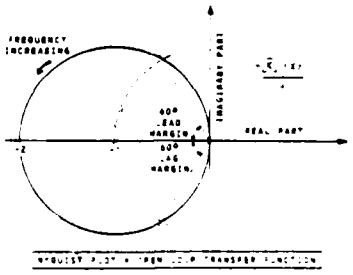

NYQUIST PLOT = OPEN LOOP TRANSFER FUNCTION

FIG.8

NYQUIST PLOT AT 1.7QF

INPUT: $\delta_{L.E.}$ ACTUATOR
OUTPUT: J_1MO/F + J_2MO/F + J_3MO/A + J_4QO/A
$J_1 \rightarrow J_4$ FROM LEAST SQUARES FIT OF TO D.O.F. WITH ACTUATOR TO IDEAL CIRCLE USING PARTIAL INTEGRATION:

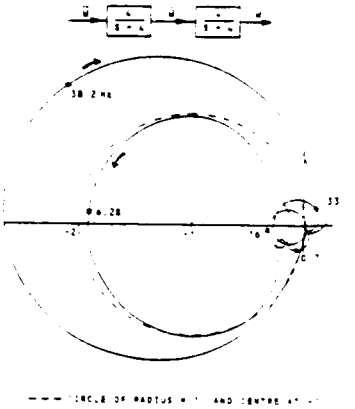

— — — CIRCLE OF RADIUS = 1 AND CENTRE AT -1

FIG.11

PRACTICAL ACTIVE FLUTTER CONTROL LAW

- DESIGN DYNAMIC PRESSURE = 1.7QF
- $\{\dot{x}\} = [S]\{x\} + [B]\{\bar{k}_1 \quad \bar{k}_2 + k_3 f_3(\omega)\}$
  k_1, $k_3 f_3(\omega)$ ARE ACTUATOR INPUT AND TRANSFER FUNCTION
- WIND TUNNEL MODEL:
  1) BINARY FLUTTER MECHANISM (BANDWIDTH 5 TO 7Hz)
  2) OTHER MODES HIGHER THAN 14Hz

$\therefore$ CONTROL LAW DESIGNED FOR BINARY SYSTEM
$\bar{k}_1 = k_1 q_1 + k_2 q_2 + k_3 q_3 + k_4 q_4$

$\therefore$ $k_1 = J_1$MO/F + J_2MO/F + J_3MO/A + J_4MO/A $\overline{f_3(\omega)}$

WHERE $\begin{matrix} MF \\ MA \end{matrix} = \begin{bmatrix} \cdots & \cdots \\ \cdots & \cdots \end{bmatrix} \begin{matrix} q_1 \\ q_2 \end{matrix}$

= DEFLECTIONS AT POSITIONS F AND A FOR BINARY

AND $\begin{bmatrix} \cdots & \cdots \\ \cdots & \cdots \end{bmatrix} = \begin{bmatrix} \cdots & \cdots \\ \cdots & \cdots \end{bmatrix}^{-1}$

FIG.9

STABILITY MARGINS

BEST CALCULATED CONTROL LAW
k_1 = J_1MO/F + J_2MO/F + J_3MO/A + J_4MO/A

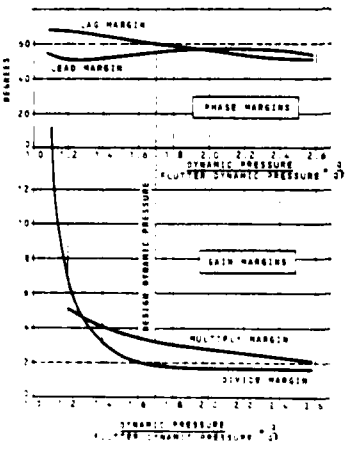

DYNAMIC PRESSURE / DESIGN DYNAMIC PRESSURE

FIG.12

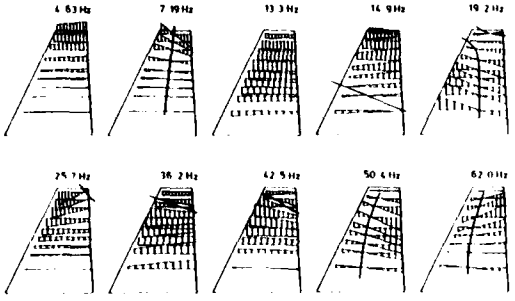

WING DEFLECTIONS IN THE COMPLETE MODEL NORMAL MODES

FIG.13

FILTER COMBINATIONS

A ACTUATOR MODEL

$$\frac{3,097,600}{(S+100)(S^2+685+30,976)}$$

B THREE SECOND ORDER FILTERS

$$\left(\frac{S^2+215+48,580}{S^2+2995+48,580}\right)\left(\frac{69,700}{S^2+264S+69,700}\right)\left(\frac{S^2+3056\cdot10}{S^2+5525+3056\cdot10}\right)$$

C FIRST HIGH PASS FILTER

$$\frac{S}{S+33}$$

D SECOND HIGH PASS FILTER

$$\frac{S}{S+10}$$

FILTER COMBINATION	FILTERS INCLUDED			
	A	B	C	D
1	✓	✓	✓	✓
2	✓	✓	✓	✓
3	✓	✓	✓	✓
4	✓	✓	✓	✓
5	✓	✓	✓	✓
6	✓	✓	✓	✓

FIG.16

Q.L.T.F. FOR L.E. ACTUATOR AND THREE VELOCITIES

TRANSDUCER POSITION	NORTHROP DATA					AFFDL DATA				
	AMPLITUDE OF FLUTTER LOBE A	GAIN MARGINS +	GAIN MARGINS −	PHASE MARGIN	GAIN PHASE	AMPLITUDE OF FLUTTER LOBE A	GAIN MARGINS +	GAIN MARGINS −	PHASE MARGIN	GAIN PHASE
OUTBOARD INBOARD 0.7	2.0	1.3	1.3	22°	65°	2.0	1.7	2.0	28°	65°
OUTBOARD AFT 0.8	2.2	1.0	1.3	22°	65°	4.0	1.0	2.3	27°	50°
OUTBOARD SLOPE 0.5	0.09	1.0	1.0	20°	52°	0.13	2.0	2.0	40°	60°

AMPLITUDE AND PHASE PROPERTIES OF ANTI-CLOCKWISE LOBE AT 1.7QF

FIG.14

FILTER DEFINITION			AMPLITUDE AT 5.72 HZ	PHASE LAG DEGREES
FIGURE 15	FIGURE 16	FILTER COMBINATION		
1			0.97	13.7
3			1.01	7.0
4			1.00	8.7
5	C		0.74	42.6
6	D		0.94	-16.0
2+3+4	B		0.86	24.3
ACTUATOR	A	3	0.96	25.9
	A+B	2	0.90	60.1
	A+B+D	4	0.92	34.6
	A+B+C	5	0.70	7.6
	A+B+C+D	6	0.88	0.6

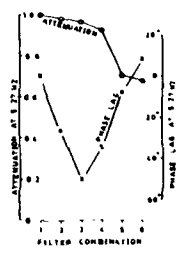

FILTER CHARACTERISTICS AT 1.7Q$_f$ FLUTTER ROOT FREQUENCY

FIG.17

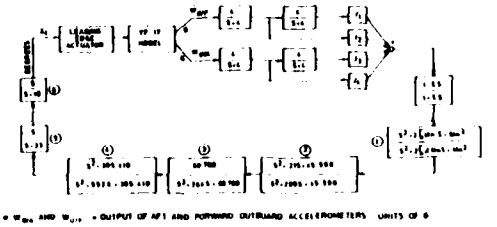

- $\ddot{w}_{aft}$ AND $\ddot{w}_{fwd}$ = OUTPUT OF AFT AND FORWARD OUTBOARD ACCELEROMETERS UNITS OF g
- ξ_c IS INPUT TO LEADING EDGE CONTROL SURFACE ACTUATOR DEGREES
- FILTERS (J) (I) AND (L) ARE TO PREVENT SERVO SYSTEM INSTABILITY
- NOTCH FILTER (J) IS TO PREVENT TIP LAUNCHER RAIL BENDING MODE INSTABILITY AT ABOUT 30Hz
- HIGH PASS FILTERS (K) AND (G) ARE TO PREVENT RIGID BODY INSTABILITY
- (I)(H) AND (E) ARE TO BE USED ONLY IF SHOWN NECESSARY DURING THE TUNNEL TESTS

ACTIVE FLUTTER CONTROL LAW

FIG.15

Q.L.T.F. FOR L.E. CONTROL AND O/A DISPLACEMENT

EVOLUTION OF ANTICLOCKWISE LOBE SHAPE WITH FILTER COMBINATION (FC) AT 1.7QF

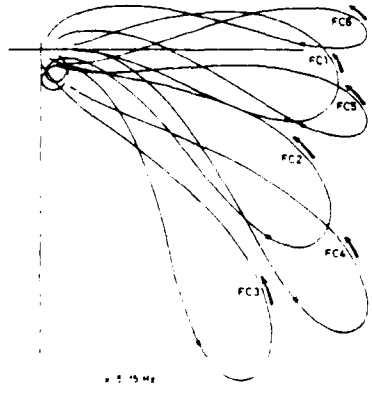

FIG.18

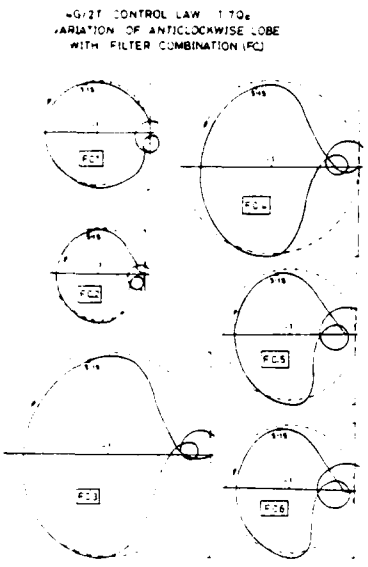

FIG.19

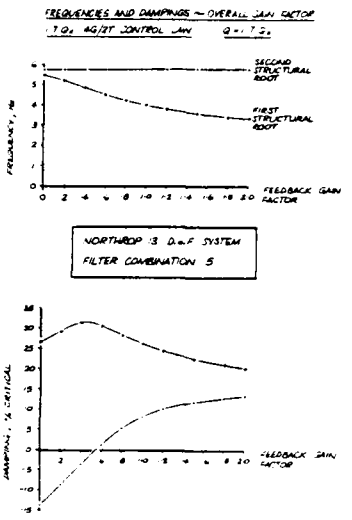

FIG.22

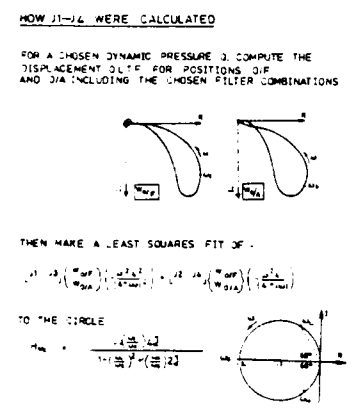

FIG.20

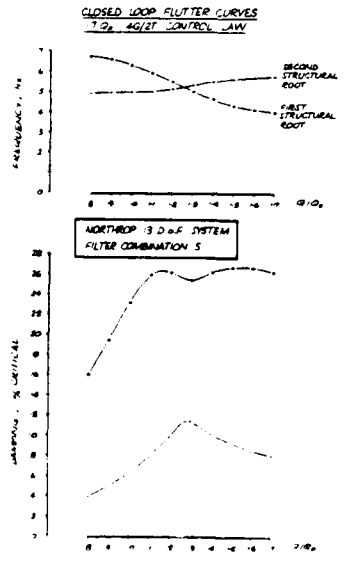

FIG.21

NORTHROP DATA L.S.F WITH ALL FILTERS
17 QF GAINS AT 17QF

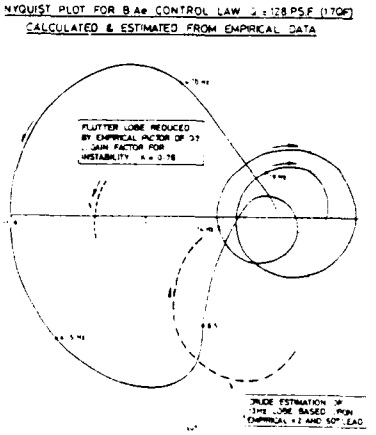

FIG.23

REPORT DOCUMENTATION PAGE

1. Recipient's Reference	2. Originator's Reference	3. Further Reference	4. Security Classification of Document
	AGARD-R-689	ISBN 92-835-0270-2	UNCLASSIFIED

5. Originator Advisory Group for Aerospace Research and Development
North Atlantic Treaty Organization
7 rue Ancelle, 92200 Neuilly sur Seine, France

6. Title REPORT ON A COOPERATIVE PROGRAMME ON ACTIVE FLUTTER SUPPRESSION

7. Presented at the 50th Structures and Materials Panel Meeting held in Athens, Greece, April 1980.

8. Author(s)/Editor(s) Various

9. Date August 1980

10. Author's/Editor's Address Various

11. Pages 56

12. Distribution Statement This document is distributed in accordance with AGARD policies and regulations, which are outlined on the Outside Back Covers of all AGARD publications.

13. Keywords/Descriptors

YF-17 (aircraft)	External stores
Fighter aircraft	Aerodynamic stability
Flutter	Active control
Wings	Control theory

14. Abstract

Presentations are given on the results of a cooperative programme on active flutter suppression on a dynamic model of the YF-17 aircraft. During this programme, British Aerospace, MBB, Northrop, Air Force Flight Dynamics Laboratory, NASA and ONERA cooperated in deriving control laws for active flutter suppression for one explosive wing-store flutter case of the model. Phase control laws were all tested and compared during wind tunnel tests performed in the Langley 16 ft wind tunnel in October 1979. Results were quite promising and open the way for future cooperation on full-scale aircraft.

AGARD Report No.689 Advisory Group for Aerospace Research and Development, NATO REPORT ON A COOPERATIVE PROGRAMME ON ACTIVE FLUTTER SUPPRESSION Published August 1980 56 pages Presentations are given on the results of a cooperative programme on active flutter suppression on a dynamic model of the YF-17 aircraft. During this programme, British Aerospace, MBB, Northrop, Air Force Flight Dynamics Laboratory, NASA and ONERA cooperated in deriving control laws for active flutter suppresion for one explosive wing-store flutter case of the model. Phase control laws were all tested and compared during P.T.O.	AGARD-R-689 YF-17 (aircraft) Fighter aircraft Flutter Wings External stores Aerodynamic stability Active control Control theory	AGARD Report No.689 Advisory Group for Aerospace Research and Development, NATO REPORT ON A COOPERATIVE PROGRAMME ON ACTIVE FLUTTER SUPPRESSION Published August 1980 56 pages Presentations are given on the results of a cooperative programme on active flutter suppression on a dynamic model of the YF-17 aircraft. During this programme, British Aerospace, MBB, Northrop, Air Force Flight Dynamics Laboratory, NASA and ONERA cooperated in deriving control laws for active flutter suppresion for one explosive wing-store flutter case of the model. Phase control laws were all tested and compared during P.T.O.	AGARD-R-689 YF-17 (aircraft) Fighter aircraft Flutter Wings External stores Aerodynamic stability Active control Control theory
AGARD Report No.689 Advisory Group for Aerospace Research and Development, NATO REPORT ON A COOPERATIVE PROGRAMME ON ACTIVE FLUTTER SUPPRESSION Published August 1980 56 pages Presentations are given on the results of a cooperative programme on active flutter suppression on a dynamic model of the YF-17 aircraft. During this programme, British Aerospace, MBB, Northrop, Air Force Flight Dynamics Laboratory, NASA and ONERA cooperated in deriving control laws for active flutter suppresion for one explosive wing-store flutter case of the model. Phase control laws were all tested and compared during P.T.O.	AGARD-R-689 YF-17 (aircraft) Fighter aircraft Flutter Wings External stores Aerodynamic stability Active control Control theory	AGARD Report No.689 Advisory Group for Aerospace Research and Development, NATO REPORT ON A COOPERATIVE PROGRAMME ON ACTIVE FLUTTER SUPPRESSION Published August 1980 56 pages Presentations are given on the results of a cooperative programme on active flutter suppression on a dynamic model of the YF-17 aircraft. During this programme, British Aerospace, MBB, Northrop, Air Force Flight Dynamics Laboratory, NASA and ONERA cooperated in deriving control laws for active flutter suppresion for one explosive wing-store flutter case of the model. Phase control laws were all tested and compared during P.T.O.	AGARD-R-689 YF-17 (aircraft) Fighter aircraft Flutter Wings External stores Aerodynamic stability Active control Control theory

wind tunnel tests performed in the Langley 16 ft wind tunnel in October 1979. Results were quite promising and open the way for future cooperation on full-scale aircraft.

Papers presented at the 50th Sturctures and Materials Panel Meeting held in Athens, Greece, April 1980.

ISBN 92-835-0270-2

wind tunnel tests performed in the Langley 16 ft wind tunnel in October 1979. Results were quite promising and open the way for future cooperation on full-scale aircraft.

Papers presented at the 50th Sturctures and Materials Panel Meeting held in Athens, Greece, April 1980.

ISBN 92-835-0270-2

wind tunnel tests performed in the Langley 16 ft wind tunnel in October 1979. Results were quite promising and open the way for future cooperation on full-scale aircraft.

Papers presented at the 50th Sturctures and Materials Panel Meeting held in Athens, Greece, April 1980.

ISBN 92-835-0270-2

wind tunnel tests performed in the Langley 16 ft wind tunnel in October 1979. Results were quite promising and open the way for future cooperation on full-scale aircraft.

Papers presented at the 50th Sturctures and Materials Panel Meeting held in Athens, Greece, April 1980.

ISBN 92-835-0270-2